REVIEWS OF TOPICAL PROBLEMS

Optics of nonstationary media

A B Shvartsburg

Contents

Abstract. Propagation and reflection of electromagnetic waves in time-varying dielectric media are studied using analytic solutions of the relevant Maxwell equations. Exactly solvable models that do not involve any requirements of small or slow changes in the medium reveal strong nonstationarity-induced dispersion effects due to a finite relaxation time of the dielectric parameters. The generalized time-dependent Fresnel and Snell laws visualizing the dependence of reflection coefficients on the dynamics of reflecting media are presented. The drastic distortion of EM fields interacting with rapidly ionizing plasmas is examined. The coupled spatiotemporal reshaping of wave fields in heterogeneous time-varying media is considered for transmission lines, heterogeneous dielectrics, and flash ionization in microwave cavities. The efficiency of the time-domain approach in treating these problems is demonstrated.

A B Shvartsburg Science and Technology Center of Unique Instrumentation, Russian Academy of Sciences,
ul. Butlerova 15, 117342 Moscow, Russian Federation
Tel. (7-095) 316 17 28
E-mail: alexshvarts@mtu-net.ru

1. Introduction. Unharmonic alternating electromagnetic fields

This review is devoted to the physical fundamentals and mathematical basis of optics of media with time-varying electromagnetic properties. These problems are currently attracting growing attention in optoelectronics, microwave physics, and the dynamics of laboratory and space plasmas. Fast variations of dielectric parameters of continuous media in the course of laser pump-probe experiments, phase transitions, and ionization processes are characterized by finite relaxation times that can become comparable to the period of the probing wave. These relaxation times determine the nonstationarity-induced dispersion of the dielectric permeability $\varepsilon(t)$, which essentially affects the spectra of reflected and transmitted radiation. The variable velocity of electromagnetic wave propagation in such media can result in a complete reshaping of both reflected and refracted waves, rapidly transforming harmonic fields to unharmonic ones. The dynamics of nonstationary electromagnetic fields opens many opportunities for optimizing processes of energy and information transfer through these media. The ongoing interest in such problems is fueled by several research goals:

— to find the time-dependent generalizations of Fresnel and Snell laws, not restricted by any assumptions about the smallness or slowness of variations of fields or media;

— to visualize the coupling between spatial and temporal variations of fields;

— to reveal methods for the fast nondestructive optical testing of materials and targets.

Moreover, an important task is to elaborate an analytic approach to these topics, which until recently were considered the exclusive field of computer simulations.

In this review, to provide some physical insight into the electromagnetic processes in media with time-dependent dielectric parameters, we consider the simplest case where the relaxation dynamics of the medium is governed not by the field of a traveling wave but by external sources, e.g., by heating, ionization, or phase transitions. This approach was used in the first attempts to explain the cross-modulation of radiowaves in the ionosphere, arising when the probing wave was traversing the plasma area with oscillating absorption, and produced due to the heating of this area by a strong field [1]. The effects of velocity modulation for HF microwaves in a transmission line with time-varying parameters were shown in Ref. [2] as long ago as 1958. Several years later, the development of laser physics attracted attention to the dynamics of optical processes in media with extremely short relaxation times of the dielectric permeability, comparable with the periods of light waves; series of such problems were posed due to the analysis of ultrafast ionization in gases [3] and solids [4]. The drastic amplitude – phase reshaping of short optical pulses interacting with these materials impedes the feasibility of traditional analysis of these interactions in the framework of the concept of harmonic alternating electromagnetic fields.

Other mechanisms for the formation of unharmonic waves are connected with the nonstationary diffraction pattern of wave pulses. The passage of a short pulse through an opening can result in its angular splitting [5] or in far-zone formation of the pulse with an envelope close to the time derivative of its initial envelope [6]. The dynamics of unharmonic single-cycle transients in a free space is now arousing interest due to perspectives of attosecond optics [7].

The mathematical formalism of electrodynamics of nonstationary media began its development as a generalization of some existing models of wave propagation in stationary heterogeneous media. One of the first papers devoted to wave propagation in a transmission line with a time-dependent velocity $v(t) = v_0 U(t)$ [2] was based on the model $U(t) = 1 + t/t_0$, similar to the well-known Rayleigh profile of a coordinate-dependent wave velocity in a heterogeneous medium, $v(z) = v_0(1 + z/L)$ [8]. The model of step-like variation of the dielectric permeability $\varepsilon(t)$ [9] was used for the presentation of complicated dependences $\varepsilon(t)$ by means of sequences of step-like changes [10], resembling the scheme of formal replacement of a continuous spatially heterogeneous distribution $\varepsilon(z)$ by some stepped profile [11]. The reflectivity of a nonstationary dielectric with $\varepsilon(t)$ given by the temporal analog of the Epstein heterogeneous layer was examined in Ref. [12]. This spatiotemporal analogy proves to be a useful tool for solving the series of problems discussed below. A formal analogy between some equations in optics of time-dependent media and electrodynamics of nonstationary transmission lines is also widely used.

This review is organized as follows. Section 2 is devoted to the time variations of cavity eigenmodes due to rapid ionization of gas inside the cavity. The exact analytic solutions of Maxwell equations for the electromagnetic waves propagating both in the dielectric medium with a time-varying refractive index $n(t)$ and in plasmas with a time-varying electron density $N(t)$ are found in Section 3.

These exactly solvable models, containing several free parameters, visualize the influence of finite relaxation times of the aforesaid variations on the reflectivity of such media. The generalized Fresnel and Snell formulas, obtained in the framework of these models for arbitrary frequencies, polarizations, and incidence angles of reflecting waves are examined in Section 4. Some peculiarities of wave dynamics in spatially heterogeneous nonstationary structures and media with time-dependent absorption are shown in Sections 5 and 6, respectively. The tendencies of the coupled space – time evolution of short unharmonic pulses are noted in Section 7; some important unsolved problems of the topic discussed are listed at the end of this section.

2. Flash ionization in the cavity and the dynamics of eigenmodes

Amplitude – frequency variations of eigenmodes in a cavity, produced by the ionization of neutral gas inside this cavity, have received considerable attention lately in the electrodynamics of time-varying media and the physics of laser – plasma interactions. These nonstationary phenomena are governed by space – time variations of the plasma frequency Ω_p, determined by the structure of ionization fronts. The simplest cases examined below are connected with the model of the sudden ionization of a neutral gas filling the cavity by a high-voltage discharge, laser pulse, or electron beam. Such sudden or 'flash' ionization leads to a reduction in the dielectric constant ε, nearly equal to one, to the value $\varepsilon = 1 - \Omega_p^2 \omega^{-2}$. This reduction provides the up-shift of the cavity eigenfrequencies and changes in eigenmode intensities.

Frequency up-conversion for the microwave radiation interacting with a layer of rapidly growing ionization density was examined in Refs [13, 14]. This nonstationary effect results in the formation of up-shifted spectra of eigenmodes $\omega_\infty = (\omega_n^2 + \Omega_p^2)^{1/2}$ [15], where ω_n is the eigenfrequency of the nth mode in the cavity filled by a neutral gas. For simplicity, we consider a rectangular cavity below. The eigenfrequencies of such a cavity with perfectly reflecting walls are known to be

$$\omega_n = \pi c \sqrt{\left(\frac{p}{L_x}\right)^2 + \left(\frac{g}{L_y}\right)^2 + \left(\frac{j}{L_z}\right)^2}, \quad (2.1)$$

where L_x, L_y, and L_z are the cavity dimensions and p, g, and j are nonnegative integers, labeled as $n = (p, g, j)$.

The electric field $\mathbf{E}(\mathbf{r}, t)$ in the cavity is determined by the equation [16]

$$\nabla^2 \mathbf{E} - \frac{1}{c^2} \frac{\partial^2 \mathbf{E}}{\partial t^2} = \frac{\Omega_p^2(\mathbf{r}, t)}{c^2} \mathbf{E}. \quad (2.2)$$

It is assumed in deriving Eqn (2.2) that plasma electrons are created with zero initial velocity. The general solution of (2.2) can be written as a linear superposition of cavity eigenmodes,

$$\mathbf{E}(\mathbf{r}, t) = \sum_n \psi_n \mathbf{E}_n(\mathbf{r}), \quad (2.3)$$

where $\mathbf{E}_n(\mathbf{r})$ describes the spatial structure of these cavity orthogonal eigenmodes:

$$\int_V \mathbf{E}_n(\mathbf{r}) \mathbf{E}_{n'}(\mathbf{r}) \, \mathrm{d}\mathbf{r} = \delta_{nn'}. \quad (2.4)$$

Here, the integration covers the entire volume V of the cavity. Substituting (2.3) in (2.2) and taking orthogonality condition (2.4) into account, we can derive an evolution equation for the mode amplitudes ψ_n,

$$\frac{\partial^2 \psi_n}{\partial t^2} + (\omega_n^2 + C_{nn})\psi_n = - \sum_{n \neq n'} C_{nn'}\psi_{n'}(t), \qquad (2.5)$$

where the mode coupling coefficients $C_{nn'}$ are given by [17]

$$C_{nn'} = \int_V \Omega_p^2(\mathbf{r}, t) E_n E_{n'} \, d\mathbf{r}. \qquad (2.6)$$

As can be clearly seen from (2.5), the different eigenmodes are linearly coupled to each other and oscillate with a time-varying frequency Ω_n defined by

$$\Omega_n^2 = \omega_n^2 + C_{nn'}. \qquad (2.7)$$

The eigenfrequencies ω_n are given in (2.1).

The simplest model for flash ionization in a cavity corresponds to the assumption that ionization occurs uniformly in the entire volume V. This means that the plasma frequency is independent of the spatial coordinates, $\Omega_p^2 = \Omega_p^2(t)$. In this case, the coupling coefficients are

$$C_{nn'} = \Omega_p^2 \delta_{nn'} \qquad (2.8)$$

and the right-hand side of (2.5) is reduced to zero. This means that the cavity modes in a homogeneous immobile time-varying media are uncoupled. Precisely this case is considered below in Sections 2.1 and 2.2, devoted to aperiodic and nonmonotonic variations of ionization density. In contrast, Section 2.3 illustrates the simplest case of spatially heterogeneous ionization produced by an ionization front moving with a constant velocity.

2.1 Monotonic saturation of ionization

Because the eigenmodes in a cavity filled by a spatially uniform plasma are uncoupled, we can solve Eqn (2.5) for each mode separately. The time dependence of the plasma frequency can therefore be presented without any loss of generality in the form
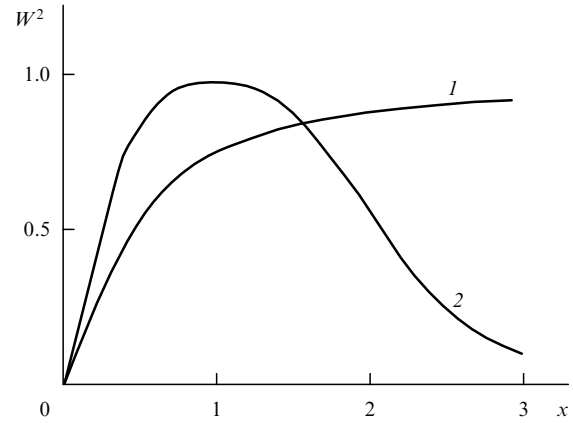
$$\Omega_p^2(t) = \Omega_0^2 W^2(t), \qquad (2.9)$$

$$W^2(t) = 1 - U^2(t), \qquad U\big|_{t=0} = 1.$$

According to (2.9), the plasma frequency grows from $\Omega_p = 0$ at the beginning of ionization ($t = 0$) up to its maximum value $\Omega_p = \Omega_0$. Substitution of (2.9) in (2.5) yields a dimensionless equation governing the evolution of the nth mode (2.1),

$$\frac{\partial^2 \psi_n}{\partial t^2} + \psi_n\{\omega_n^2 + \Omega_0^2[1 - U^2(t)]\} = 0. \qquad (2.10)$$

Omitting the index n for simplicity, introducing the new function $F = \psi\sqrt{U}$,

$$\frac{\partial^2 F}{\partial t^2} - \frac{U_t}{U}\frac{\partial F}{\partial t} + F\left[\omega_n^2 + \Omega_0^2(1 - U^2) + \frac{3}{4}\frac{U_t^2}{U^2} - \frac{U_{tt}}{2U}\right] = 0, \qquad (2.11)$$

and using the new variable

$$\tau = \int_0^t U(t') \, dt', \qquad (2.12)$$

we can eliminate the term with the first derivative $\partial F/\partial t$ from (2.11),

$$\frac{\partial^2 F}{\partial \tau^2} + F\left[\frac{\omega_\infty^2}{U^2(\tau)} - \Omega_0^2 + \frac{U_\tau^2}{U^2} - \frac{U_{\tau\tau}}{2U}\right] = 0, \qquad (2.13)$$

$$\omega_\infty^2 = \omega_n^2 + \Omega_0^2.$$

The model dependence $U(t)$ has not been specified yet and, thus, Eqn (2.13) is used below for the different models of $U(t)$.

We first consider the monotonic dependence characterized by only one free parameter, the time scale t_0:

$$U(t) = \left(1 + \frac{t}{t_0}\right)^{-1}. \qquad (2.14)$$

The instant $t = 0$ corresponds to the beginning of ionization; the saturation of ionization ($U \to 0$, $\Omega_p \to \Omega_0$) sets in for the times $t \gg t_0$ (Fig. 1). Substitution of (2.14) in (2.12) gives the explicit expressions for the new variable τ and the function $U(\tau)$,

$$\tau = t_0 \ln\left(1 + \frac{t}{t_0}\right), \qquad U(\tau) = \exp\left(-\frac{\tau}{t_0}\right). \qquad (2.15)$$

Introducing the new variable $\delta = U^{-1}$, we can rewrite master equation (2.13) in the form of a Bessel equation:

$$\frac{\partial^2 F}{\partial \delta^2} + \frac{1}{\delta}\frac{\partial F}{\partial \delta} + F\left(\omega_\infty^2 t_0^2 - \frac{q^2}{\delta^2}\right) = 0, \qquad (2.16)$$

$$q^2 = (\Omega_0 t_0)^2 + \frac{1}{4}.$$

Solution of Eqn (2.16) is given by the Hankel function $H_q^{(2)}$.

Figure 1. Normalized density of ionization $W^2(t) = N(t)/N_0$ is plotted vs the normalized time $x = t/t_0$. Curve *1* relates to the monotonic saturation (2.14), curve *2* — to nonmonotonic variations W^2; the ascending and descending parts of curve *2* are presented by models (2.20) and (2.42) for the cases $0 \leqslant t \leqslant t_m$ and $t \geqslant t_m$, respectively.
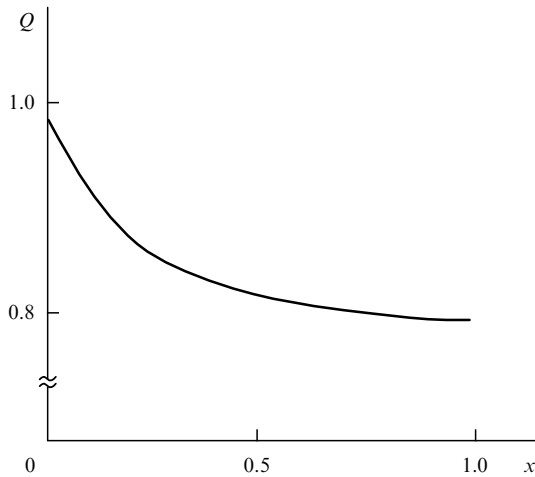
Figure 2. Time variations of the fundamental eigenmode intensity due to flash ionization in the cavity for saturation of ionization (2.14). The normalized intensity of the electric component Q of this mode is plotted vs the normalized time $x = t/t_0$, $(\Omega_{\mathrm{p}} t_0)^2 = 0.75$, $\Omega_{\mathrm{p}} = \sqrt{3}\,\omega_0$.

Finally, using (2.12), we obtain the time-dependent part of the nth eigenmode of nonstationary electric field (2.3),

$$\psi_n = A_n \sqrt{1 + \frac{t}{t_0}}\, H_q^{(2)}\left[\omega_\infty t_0 \left(1 + \frac{t}{t_0}\right)\right], \tag{2.17}$$

where the function $H_q^{(2)}$ is chosen in order to provide the asymptotic time dependence of the solution described for long times $t \gg t_0$ by harmonic oscillations $\exp\left(-\mathrm{i}\omega_\infty t\right)$, and A_n is a normalization constant. Supposing the stationary oscillations of eigenmodes with amplitudes A_{n0} to be fixed at the time instant $t = 0$, we can write the constant A_n as

$$A_n = A_{n0}\left[H_q^{(2)}(\omega_\infty t_0)\right]^{-1}. \tag{2.18}$$

Substitution of (2.18) in (2.17) gives the expression describing the unharmonic oscillations of the electric field accompanying the process of growing ionization. This result is not restricted by any assumptions about the values of the cavity eigenfrequencies ω_n, plasma frequency Ω_0, or ionization time scale t_0. The asymptotic form of the Hankel function for large values of the argument gives the expression for the electric field in the limit $t \gg t_0$, when the steady state of the ionization process is nearly achieved:

$$\psi_n = \frac{A_{n0}}{H_q^{(2)}(\omega_\infty t_0)} \sqrt{\frac{\pi}{2(\omega_\infty t_0)}} \exp\left[-\mathrm{i}(\omega_\infty t + \varphi_n)\right], \tag{2.19}$$

$$\varphi_n = \omega_\infty t_0 - \frac{\pi}{4} - \frac{\pi}{2}\,q.$$

Owing to ionization in the cavity, the eigenfrequencies grow from ω_n up to ω_∞ and the amplitudes of eigenmodes can be reduced; this effect for the intensity of the electric component is illustrated in Fig. 2. The authors of [18] link such a reduction to the collisionless plasma heating produced by the forming plasma waves. A similar decrease in the electric field was reported in the framework of the WKB approximation in Ref. [19] for the model $U = \exp\left(-t/t_0\right)$. Both these models are characterized by one free parameter, the time scale t_0 determining the growth of the electron

density at the beginning of the ionization process. More complicated models of flash ionization, containing two free parameters, are considered below.

2.2 Nonmonotonic ionization

We consider the nonmonotonic process of ionization, when the electron density first grows up to its maximum value during some finite time T and then either begins to decrease or remains constant. The dynamics of eigenmodes in the cavity is governed by Eqn (2.10), but the ascending branch of the function $U(t)$ is presented here by the more flexible model containing two free parameters: the characteristic time scale t_0 and a dimensionless number M:

$$U^2(t) = \left(\cos\frac{t}{t_0} + M\sin\frac{t}{t_0}\right)^{-2}, \tag{2.20}$$

$$M \geqslant 0, \quad U^2\big|_{t=0} = 1, \quad U^2\big|_{t=T} = (1 + M^2)^{-1} = U_{\mathrm{m}}^2. $$

The parameters t_0 and M are determined by the initial rate of ionization growth t_1 and the time T:

$$\frac{\partial U^2}{\partial t}\bigg|_{t=0} = -\frac{2M}{t_0} = -\frac{1}{t_1}, \quad \frac{\partial U^2}{\partial t}\bigg|_{t=T} = 0, \tag{2.21}$$

$$t_0 = T(\arctan M)^{-1}. \tag{2.22}$$

The solution of Maxwell equation (2.10) for the model in (2.20), shown in Fig. 1, can be obtained by means of the procedure described in Section 2.1. Performing transformations (2.11), we obtain Eqn (2.13), but with the parameter ω_∞ different from the one in (2.13):

$$\omega_\infty^2 = \omega_n^2 + \Omega^2, \quad \Omega^2 = \Omega_0^2(1 + M^{-2}). \tag{2.23}$$

Substitution of (2.20) in (2.12) yields the new variable τ,

$$\tau = \frac{t_0}{\sqrt{1 + M^2}} \ln \frac{1 + m_+ \tan\left(t/(2t_0)\right)}{1 - m_- \tan\left(t/(2t_0)\right)}, \tag{2.24}$$

$$m_\pm = \sqrt{1 + M^2} \pm M, \quad m_+ m_- = 1. \tag{2.25}$$

Using (2.24) and (2.20), we can obtain the explicit expression for $U(\tau)$:

$$U(\tau) = \frac{\cosh\varphi}{\sqrt{1 + M^2}}, \quad \varphi = \frac{\tau\sqrt{1 + M^2}}{t_0} - \mathrm{arsinh}\, M, \tag{2.26}$$

$$\varphi\big|_{t=0} = \varphi_0 = -\ln(m_+), \quad \varphi\big|_{t=T} = 0. \tag{2.27}$$

Finally, substitution of (2.23) and (2.26) in Maxwell equation (2.13) gives the equation governing the function F:

$$\frac{\partial^2 F}{\partial\varphi^2} + F\left(-q^2 + \frac{D}{\cosh^2\varphi}\right) = 0, \tag{2.28}$$

$$D = (\omega_\infty t_0)^2 - \frac{1}{4}, \quad q^2 = \frac{1}{4} + \frac{(t_0\Omega_0)^2}{M^2}. \tag{2.29}$$

Equation (2.28) is well known in quantum mechanics [20]. It is worth emphasizing that in contrast to the traditional quantum mechanics, Eqn (2.28) is written in the φ-space.

To solve Eqn (2.28), it is useful to introduce a new function f and a new variable u:

$$f = F(\cosh \varphi)^q, \qquad u = \frac{1}{2}(1 - \tanh \varphi). \tag{2.30}$$

By these transformations, Eqn (2.28) is reduced to the standard hypergeometric equation

$$u(1 - u)\frac{\partial^2 f}{\partial u^2} - \left[\gamma - u(1 + \alpha + \beta)\right]\frac{\partial f}{\partial u} - \alpha\beta f = 0, \tag{2.31}$$

$$\alpha, \beta = \frac{1}{2} + q \pm \omega_\infty t_0, \qquad \gamma = 1 + q, \tag{2.32}$$

where the value of q is determined in (2.29). Because the parameters in (2.32) satisfy the condition

$$\alpha + \beta + 1 = 2\gamma, \tag{2.33}$$

solutions of Eqn (2.31) are known to be the hypergeometric functions [18]

$$f_1 = f(\alpha, \beta, \gamma, u), \qquad f_2 = f(\alpha, \beta, \gamma, 1 - u). \tag{2.34}$$

Now, we can write the electric field in (2.11) in a form convenient for the forthcoming analysis. Presenting the factor $U^{-1/2}$ in (2.11) by means of (2.26) as

$$U^{-1/2} = \sqrt[4]{1 + M^2}\,(\cosh \varphi)^{-1/2} \tag{2.35}$$

and using (2.30) and (2.34), we obtain the solutions of (2.10) for the nth eigenmode:

$$\psi_{1,2} = A\sqrt[4]{1 + M^2}\,f_{1,2}(\cosh \varphi)^{-1/2-q}. \tag{2.36}$$

With the values of the parameters α and β given in (2.32), we can choose a linear superposition of solutions f_1 and f_2 in (2.36) such that it ensures a decrease in the eigenmode amplitude at the beginning of ionization.

This analysis is valid for arbitrary correlations between the frequencies ω_n and Ω_0 and the parameters t_0 and M. However, for some values of these quantities, the obtained results can be simplified due to the reduction of hypergeometric functions to elementary ones. Thus, in the case where

$$\beta = \frac{1}{2} + q - \omega_\infty t_0 = -m, \qquad m = 0, 1, 2, \ldots, \tag{2.37}$$

the hypergeometric function is known to be reduced to an nth-degree polynomial [20]; for example, in the simple case where $n = 0$, Eqn (2.36) yields

$$f_1 = f_2 = 1, \qquad A = (1 + M^2)^{q/2}A_0,$$
$$\left.\frac{\partial \psi}{\partial t}\right|_{t=0} = Mt_0^{-1}\left(\frac{1}{2} + q\right). \tag{2.38}$$

The condition

$$\left.\frac{\partial \psi}{\partial t}\right|_{t=0} < 0$$

is satisfied if $q < -1/2$, and we therefore have to choose the minus sign in the square root defining the value of q from (2.29). The amplitude ψ then decreases monotonically,

achieving the value

$$\left.\psi\right|_{t=T} = A_0(1 + M^2)^{q/2+1/4} < A_0 \tag{2.39}$$

at the instant of maximum ionization ($t = T$).

Another simple solution of Eqn (2.28) arises in the case where $D = 0$, $\omega_\infty t_0 = 0.5$. Using the definition of φ_0 in (2.27), we obtain

$$\psi = \frac{A_0\sqrt[4]{1 + M^2}\,\exp\left[q(\varphi_0 - \varphi)\right]}{\sqrt{\cosh \varphi}}, \qquad \left.\psi\right|_{t=T} = \frac{A_0\sqrt[4]{1 + M^2}}{(m_+)^q},$$
$$\left.\frac{\partial \psi}{\partial t}\right|_{t=0} = A_0 t_0^{-1}\left(\frac{M}{2} - q\sqrt{1 + M^2}\right). \tag{2.40}$$

In contrast to the previous case, the derivative $\partial\psi/\partial t|_{t=0}$ is negative for $q > 1/2$. Therefore, solution (2.40) describes a monotonic decrease of the electric field amplitude from $\psi(0)$ to $\psi(T)$,

$$\frac{\psi(T)}{\psi(0)} = \frac{\sqrt[4]{1 + M^2}}{(m_+)^q} < 1. \tag{2.41}$$

Depending on the cavity eigenfrequencies and the parameters of the ionization process, this decrease may become rather substantial. Presentation of the descending branch of ionization density by means of the model

$$\left.W^2(t)\right|_{t \geqslant T} = \cosh^{-2}\left(\frac{t - T}{t_2}\right) \tag{2.42}$$

yields a continuous dependence of the plasma frequency $\Omega_p(t)$ and its first time derivative at the instant of maximum ionization $t = T$ for arbitrary values of the time scale t_2. To provide the continuity of the second derivative of the plasma frequency at the same instant $t = T$, the value of t_2 has to be chosen as

$$t_2 = Mt_0. \tag{2.43}$$

Thus, models (2.20) and (2.42) describe the time-dependent ionization for each time $0 \leqslant t < \infty$ (see Fig. 1).

The Maxwell equation for an electric field in the cavity with decreasing ionization density (2.42) can be written in the form similar to (2.28),

$$\frac{\partial^2 \psi_n}{\partial t^2} + \psi_n\left[\omega_n^2 + \frac{\Omega_0^2}{\cosh^2\left[(t - T)/t_2\right]}\right] = 0. \tag{2.44}$$

Using this analogy, we can express the solution of (2.44) through hypergeometric functions f_1 and f_2:

$$\psi = (\cosh x)^{-iq}\left[Af_1(x) + Bf_2(x)\right], \tag{2.45}$$

where A and B are some constants,

$$q = \omega_n t_2, \qquad D = (\Omega_0 t_2)^2, \qquad x = \frac{t - T}{t_2}. \tag{2.46}$$

The parameters of these hypergeometric functions are

$$\alpha, \beta = \frac{1}{2} + iq \pm \sqrt{1 + 4(\omega_\infty t_2)^2}. \tag{2.47}$$

Solution (2.45) describes the growth of amplitudes due to a decrease in ionization.

The dynamics of uncoupled eigenmodes was examined here for models of spatially homogeneous ionization. However, in a more realistic situation related to spatially heterogeneous electron density or mobile ionization fronts, some coupling of modes occurs. In the next section, it is shown that this mode coupling can essentially modify the temporal modulation of eigenmodes.

2.3 Coupling of eigenmodes
due to moving ionization fronts

The up-shift of eigenfrequencies due to ionization in a cavity can be increased as compared with homogeneous ionization if the electron density is spatially heterogeneous. The time evolution of each mode proves to be coupled in this case to the evolution of all the other modes in the cavity. To visualize some salient features of this process, it is worthwhile considering flash ionization produced by an electron beam.

We assume that the electron density perturbation associated with an electron beam crosses a rectangular cavity in the z-direction with some constant velocity v. If we suppose, for simplicity, that the electron beam is homogeneous in the plane $z = 0$ and crosses the boundary $z = L_z$ at $t = 0$, moving towards $z = 0$, we can write

$$\Omega_{\mathrm{p}}^2(\mathbf{r}, t) = \Omega_0^2 f(z + vt) \,. \tag{2.48}$$

To calculate the coupling coefficients $C_{nn'}(t)$ in (2.6) for the density profile described by (2.48), we must take the orthogonality of eigenfunctions for transverse standing electromagnetic waves into account. Substitution of (2.48) in (2.6) yields

$$C_{nn'}(t) = \frac{2}{L_z} I_{nn'} \delta_{pp'} \delta_{gg'} \,, \tag{2.49}$$

$$I_{nn'} = \int_0^{L_z} \sin\left(\frac{jz}{L_z}\right) \sin\left(\frac{j'z}{L_z}\right) f(z + vt) \, \mathrm{d}z \,. \tag{2.50}$$

The simplest model for calculation of the coupling coefficients $C_{nn'}$ in (2.49) is connected with the representation of the beam density profile by means of the Heaviside function H,

$$\Omega_{\mathrm{p}}^2(z, t) = \Omega_0^2 H(z + vt - L_z) \,. \tag{2.51}$$

Substitution of (2.51) in (2.50) gives the values of the coupling coefficients [21]

$$C_{nn'}(t) = \frac{\Omega_0^2}{\pi} \delta_{pp'} \delta_{gg'} \left\{ \frac{1}{j+j'} \sin\left[\frac{\pi}{L_z}(j+j')vt\right] \right.$$
$$\left. - \frac{1}{j-j'} \sin\left[\frac{\pi}{L_z}(j-j')vt\right] \right\}, \quad j \neq j', \tag{2.52}$$

$$C_{nn'}(t) = \frac{\Omega_0^2}{2\pi j} \left\{ \frac{2\pi j}{L_z} vt + \sin\left[2\pi j\left(1 - \frac{vt}{L_z}\right)\right] \right\}, \quad j = j' \,. \tag{2.53}$$

An analysis of (2.52) and (2.53) shows that the mode coupling occurs in the geometry discussed above along the direction of perturbation propagation. Substitution of (2.52) and (2.53) in (2.5) yields a set of equations governing the evolution of coupled modes in a cavity.

This set of equations can be solved numerically [21]; however, some qualitative results can be revealed without these solutions. We assume that there is a dominant mode n_1

such that we can retain only the term corresponding to this mode in the right-hand side of (2.5),

$$a_{n1} = A_{n1} \exp\left(-\mathrm{i}\omega_{n1}t\right), \tag{2.54}$$

where A_{n1} is the amplitude of the n_1th mode. If the slow evolution of frequency ω_n is neglected, we see from (2.5) that four modes a_n can be resonantly excited. These modes satisfy the resonant condition

$$\omega_n \pm \frac{\pi n v}{L_z} = \omega_{n1} \pm \frac{\pi v n_1}{L_z} \,. \tag{2.55}$$

This resonance can be explained if we consider the dominant mode as a linear superposition of two counter-popagating waves of the same frequency and amplitude. The plus (minus) sign in the right-hand side of (2.55) refers to counter- (co-) propagation of the dominant mode with respect to the moving perturbation of the electron density. If the resonant mode n corresponds to the reflection (transmission) of the dominant mode, then the sign in the left-hand side of (2.55) must be opposite (equal) to the sign in the right-hand side of (2.55). This can easily be seen in a free space, where $K_z = \omega c^{-1}$, $K_z' = \omega' c^{-1}$, and the resonant condition (2.55) simply reduces to the double Doppler shift effect, giving the frequencies of the counter-propagating (ω') and co-propagating (ω'') waves as

$$\omega' = \frac{\omega(1+\beta)}{1-\beta} \,, \qquad \omega'' = \frac{\omega(1-\beta)}{1+\beta} \,. \tag{2.56}$$

The frequencies ω_n and ω_{n1} were supposed above to retain constant values. However, the resonant modes satisfy time-dependent dispersion equation (2.7) and therefore, rigorously speaking, some time variations of ω_n and ω_{n1} do exist. This means that several modes eventually obey resonant conditions (2.55) while the perturbation front evolves across the cavity. Moreover, the resonant frequency up-shift produced by the moving ionization front can essentially exceed the value of the up-shift in a homogeneously ionized medium, especially in the case of relativistic velocities of ionization fronts [21].

The mode coupling effects are shown to provide a broad spectrum of eigenmodes. This result is in agreement with experimental observations [22]. A similar analysis can be performed in the case where space–time variations of density are created due to photoionization of the neutral gas in a cavity [23]. All these effects are examined for standing waves in a cavity. The dynamics of traveling electromagnetic waves in semi-infinite nonstationary media are considered in Section 3 below.

3. Dynamical and adiabatic regimes
in the reflectivity of time-varying dielectrics

This section is devoted to the amplitude, phase, and frequency modulation of electromagnetic waves interacting with dielectrics with time-dependent optical properties. Such situations can be encountered in a series of 'hot' topics in the physics of laboratory and space plasmas, energy transfer through nonstationary media, and optical diagnostics of ultrafast processes. The time variations of dielectric susceptibilities are characterized by finite relaxation times, and the nonstationary reflectivity of such materials depends on the ratios of these relaxation times to periods of EM waves. Some tendencies in the processes of coupled amplitude–phase

reshaping of EM waves in nonstationary dielectrics were found in Refs [24, 25] by numerical simulations. However, analytic insights into the optics of time-varying media have been less elaborated up to now than those of heterogeneous materials.

One of the first attempts to develop an analytic approach to nonstationary electrodynamics was based on the model of a 'sudden' jump-like variation of the dielectric susceptibility [9]. This model is widely used now for analysis of up-shifting of the frequency of waves interacting with a rapidly moving ionization front in gases. Such a front, created by laser-induced ionization of a neutral gas, has an ultrashort rise time (about the half-pulse duration); the plasma characteristics behind the front change slowly in the recombination time scale ($\sim$ ns). The front propagates with the velocity v nearly equal to the group velocity of the laser pulse. Interaction of the moving front with the probe photons, provided by a secondary, low-energy laser probe pulse, results in an up-shift of its frequency. This effect, entitled *photon acceleration* in Ref. [26], ensures significant blue-shifting caused by relativistic ionization fronts [27, 28]. The frequency blue-shift attained by a probe laser pulse with the initial frequency ω_0 after collision with the front moving with the velocity v at the angle γ is [29]

$$\frac{\omega_{up}}{\omega_0} = \frac{1 - \beta \cos \gamma}{1 - \beta^2} - \frac{\beta \sqrt{(\beta - \cos \gamma)^2 - \Omega_{\rm m}^2 \omega^{-2}(1 - \beta^2)}}{1 - \beta^2} , \tag{3.1}$$

where $\Omega_{\rm m}$ is the maximum plasma frequency of the ionization front, the co- and counter-propagation configurations correspond to the respective values $\gamma = 0$ and $\gamma = \pi$, and $\beta = v/c$.

Formula (3.1) was verified in the experiments [30], which demonstrated the spectral up-shift of the order of 25 nm for the probe photons ($\lambda = 560$ nm). These phenomena attract attention due to their potential use as a diagnostic tool for the measurement of relativistic velocities of plasma structures and for the design of new types of tunable and ultrashort radiation sources [22] An essential blue-shifting of photons was shown to arise due to the collision of probe photons with the accelerated ionization fronts produced by the propagation of an ionizing laser pulse in a gas with a density gradient [31].

All these phenomena are based on the interactions of photons with moving interfaces resembling different modifications of the Doppler frequency shift. In contrast, this section is devoted to frequency variations arising due to the interaction of radiation with an immobile dielectric whose dielectric permeability varies in time. Moreover, the aforesaid examples relate to the limiting case where the relaxation time t_0 of the nonstationary dielectric permeability of the medium is much shorter than the characteristic times T of the alternating electromagnetic field. The opposite limit corresponds to the adiabatic approximation, where $T \gg t_0$. However, in a number of problems, both applied and academic, situations occur where the time scales T and t_0 prove to be of the same order of magnitude and, thus, the exact analytic solutions of Maxwell equations with time-dependent coefficients are required for the analysis of the wave dynamics. Some of these exactly solvable models are considered below.

To illustrate the crucial role of nonstationary variations of the dielectric permeability $\varepsilon(t)$, we consider the simplest case where the relaxation dynamics of the medium are governed

not by the field of the traveling wave but by external sources, e.g., by heating, ionization, or phase transitions. In particular, this approach can be related to the optics of a probing wave in the so-called 'pump-probe' experiments, involving ultrashort pump pulses.

To tackle this problem, we model a nonstationary spatially homogeneous, nonmagnetic, and lossless medium by writing the dielectric displacement $\mathbf{D}$ produced by a variable electric field $\mathbf{E}(t)$ as a scalar product

$$\mathbf{D} = \varepsilon(t)\,\mathbf{E}(t) . \tag{3.2}$$

The dielectric permeability $\varepsilon(t)$ can be expressed through the function $U(t)$ as

$$\varepsilon(t) = n_0^2 U^2(t) , \qquad U\big|_{t=0} = 1 , \tag{3.3}$$

where n_0 is the value of the refractive index before perturbation and the dimensionless function $U(t)$ accounts for the time dependence of the dielectric permeability.

To examine the reflection and refraction on the boundary $z = 0$ of the half-space filled by dielectric (3.2), (3.3) or an ionizing medium, the following problems have to be solved:

(1) to find the models of time-dependent dielectric permeabilities (3.2) and (3.3) and to obtain the relevant solutions of Maxwell equations, visualizing the crucial role of nonstationarity-induced dispersion;

(2) to build the nonstationary generalizations of Fresnel formulas describing both dynamical and adiabatic reflection regimes; and

(3) to illustrate the link between the reflectivity of the ionizing medium and the ionization times.

3.1 Dispersion of nonstationary dielectrics

The finite relaxation times of the nonstationary dielectric permeability $\varepsilon(t)$ determine the variety of regimes of propagation of an electromagnetic wave in a dielectric characterized by a time-dependent $\varepsilon(t)$. To visualize these regimes, we consider a linearly polarized EM wave, incident normal on the boundary of the half-space $z \geqslant 0$ filled by the nonstationary dielectric. The electric and magnetic components of this wave are related by the Maxwell equations

$$\frac{\partial E_x}{\partial z} = -\frac{1}{c}\frac{\partial H_y}{\partial t} , \tag{3.4}$$

$$\frac{\partial H_y}{\partial z} = -\frac{1}{c}\frac{\partial D_x}{\partial t} . \tag{3.5}$$

We have implicitly assumed that the medium is nonmagnetic; the electric displacement D_x is determined by Eqn (3.2).

Solving system (3.4), (3.5) involves three steps.

(A) We reduce this system to one equation governing the electric displacement D_x,

$$\frac{\partial^2 D_x}{\partial z^2} - \frac{n_0^2 U^2(t)}{c^2}\frac{\partial^2 D_x}{\partial t^2} = 0 . \tag{3.6}$$

Introducing the new variable τ of the dimension of time as

$$\tau = \int_0^t \frac{\mathrm{d}t'}{U(t')} \tag{3.7}$$

and the new function

$$F = \frac{D_x}{\sqrt{U(t)}} , \tag{3.8}$$

we can write Eqn (3.6) as

$$\frac{\partial^2 F}{\partial z^2} - \frac{n_0^2}{c^2}\frac{\partial^2 F}{\partial \tau^2} = \frac{n_0^2}{c^2}\, F\left[\frac{UU_{tt}}{2} - \frac{U_t^2}{4}\right]. \tag{3.9}$$

(B) The time dependence of the dielectric permeability still remains unknown. However, with the new representation in (3.7) and (3.8), the time-dependent coefficient is eliminated from the left-hand side of Eqn (3.9). The nonstationarity is now taken into account by the expression in brackets on the right-hand side of Eqn (3.9). A particularly interesting class of $U(t)$ corresponds to the simplest case where the expression in brackets in Eqn (3.9) is equal to some real constant T^{-2}; the quantity T has the dimension of time:

$$\frac{UU_{tt}}{2} - \frac{U_t^2}{4} = \frac{1}{T^2}\,. \tag{3.10}$$

The function F is then governed by an equation with constant coefficients:

$$\frac{\partial^2 F}{\partial z^2} - \frac{n_0^2}{c^2}\frac{\partial^2 F}{\partial \tau^2} = \frac{n_0^2}{c^2 T^2}\, F\,. \tag{3.11}$$

Equations (3.10) and (3.11) determine the time dependence of the dielectric permeability $U(t)$ and the wave fields corresponding to the model $U(t)$. The normalized dielectric permeability described by the solution of Eqn (3.10) satisfying the condition $U(0) = 1$ is [32]

$$U(t) = 1 + \frac{s_1 t}{t_1} + \frac{s_2 t^2}{t_2^2}\,, \qquad s_{1,2} = 0, \pm 1\,, \tag{3.12}$$

where t_1 and t_2 are positive free parameters. The constant T^{-2} can be expressed in terms of these parameters, which, in their turn, are connected with the extremum U_m and duration d of profile (3.12):

$$\frac{1}{T^2} = \frac{s_2}{t_2^2} - \frac{s_1^2}{4t_1^2}\,. \tag{3.13}$$

Depending on the values of t_1, t_2 and s_1, s_2, the function $U(t)$ provides flexible representations of both ascending and descending time dependences $U(t)$, shown in Fig. 3. For instance, in the case where $s_1 = -1$, $s_2 = 1$, and $t_2 \leqslant 2t_1$, the function $U(t)$ reaches its minimum U_m (see Fig. 3) at the instant t_m:

$$t_m = yt_2\,, \qquad U_m = U(t_m) = 1 - y^2\,, \qquad y = \frac{t_2}{2t_1} < 1\,. \tag{3.14}$$

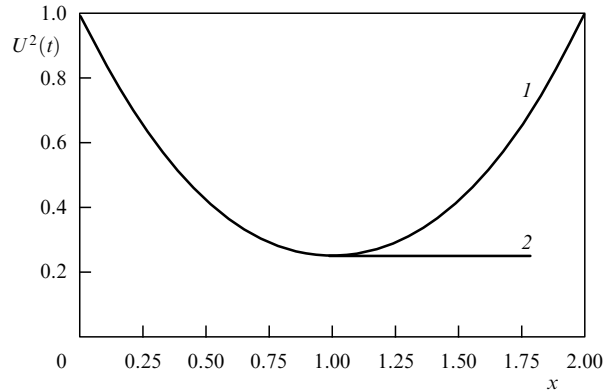At the instant $t = 2t_m$, this dielectric function returns to its initial value $U = 1$.

(C) The solution of Eqn (3.11) related to model (3.12) can be written as a traveling wave in the (z, τ)-space:

$$F = \exp\left[\mathrm{i}(qz - \omega\tau)\right]\,, \tag{3.15}$$

$$q = \frac{\omega n_0}{c}\, N\,, \qquad N = \sqrt{1 - (\omega T)^{-2}}\,.$$

Substitution of solution (3.15) in Eqn (3.8) yields the electric displacement

$$D_x = A\sqrt{U(t)}\,\exp\left[\mathrm{i}(qz - \omega\tau)\right]\,, \tag{3.16}$$

Figure 3. Time-varying normalized dielectric permeability $U^2(t)$ (3.12), $s_1 = -1$, $s_2 = 1$, $x = t/t_m < 1$; the characteristic time t_m is given in (3.14). When $x \geqslant 1$, the permeability U^2 either returns to its initial value ($U = 1$, branch *1*) or remains constant ($U = U_m$, branch *2*).

where A is a normalization constant. Finally, substitution of Eqn (3.16) in (3.5) gives the expressions for the field components inside nonstationary medium (3.12) and for the parameter τ:

$$E_x = \frac{A}{n_0^2}\left[U(t)\right]^{-3/2} \exp\left[\mathrm{i}(qz - \omega\tau)\right]\,; \tag{3.17}$$

$$H_y = \frac{A}{n_0 N}\left[U(t)\right]^{-1/2} \exp\left[\mathrm{i}(qz - \omega\tau)\right]\,; \tag{3.18}$$

$$\tau = \frac{t_2}{\sqrt{1 - y^2}}\arctan\left(\frac{t\sqrt{1 - y^2}}{t_2 - ty}\right)\,, \qquad s_1 = -1\,, \qquad s_2 = 1\,; \tag{3.19}$$

$$\tau = \frac{t_2}{2\sqrt{1 + y^2}}\ln\left[\frac{1 + t(t_2 y_-)^{-1}}{1 - t(t_2 y_+)^{-1}}\right]\,, \qquad s_1 = 1\,, \qquad s_2 = -1\,, \tag{3.20}$$

$$y_\pm = \sqrt{1 + y^2} \pm y\,.$$

Thus, using the formalism of τ-space gives the explicit expressions for the EM field, valid during the time of existence of model (3.12): $0 \leqslant t \leqslant t_2^2/t_1 = 2yt_2$. To examine the field at the time $t \geqslant 2yt_2$, we must specify the dependence $U(t)$ at this time. This specification is shown below to provide a series of peculiarities in the reflectivity of medium (3.12) at the instant $t = t_m$.

The formulas for EM fields (3.17) and (3.18) propagating in nonstationary medium (3.12) are obtained without any restricting assumptions about the relations between the frequency and the relaxation times of the medium t_1 and t_2. These formulas contain the phase factor $\exp\left[\mathrm{i}(qz - \omega\tau)\right]$, expressed using the variable τ: in this 'τ-space', the spatio-temporal structure of the discussed EM fields resembles that of traveling harmonic waves.

We next analyze the amplitude – phase structure of field components (3.17) and (3.18), emphasizing some peculiarities of this structure originating from the strong nonstationarity of the medium in which they travel.

(1) The wave propagation is characterized by the non-stationarity-induced dispersion described by the factor q in Eqn (3.15). This effect, independent of the natural dispersion of material, is determined by the relaxation times of the variable dielectric permeability. The concave temporal profile of dielectric permeability depicted in Fig. 3 gives rise

to the normal dispersion

$$N = \sqrt{1 - (\omega T)^{-2}} \, .$$

This waveguide-like formula shows the appearance of a nonstationarity-induced cutoff frequency $\omega_c = T^{-1}$. In contrast, a convex profile of $U(t)$ gives rise to the abnormal dispersion

$$N = \sqrt{1 + (\omega T)^{-2}} \, ,$$

and the cutoff effect does not arise in this case.

(2) The propagation of an EM wave in a nonstationary dielectric, described in terms of the τ-space, is accompanied by the formation of time-dependent phase shift φ between the E_x and H_y components. Substitution of (3.12) in (3.18) gives the value of this phase shift:

$$\varphi = \arcsin \left[\frac{y s_1 + s_2 t / t_2}{\sqrt{(\omega t_2)^2 + (s_1 y + s_2 t / t_2)^2}} \right] . \tag{3.21}$$

In the (z, t)-space, the waveforms of electric and magnetic components (3.17) and (3.18) are nonsinusoidal and, moreover, owing to time-varying factor (3.21), these waveforms are different in each cross section inside the medium.

(3) The time scales t_1 and t_2, as well as the values s_1 and s_2, are free parameters of model (3.12). In the special case where $t_2 = 2t_1$, $s_1 = \pm 1$, $s_2 = 1$, the nonstationarity-induced dispersion vanishes ($N = 1$, $T \to \infty$) and the time-dependent factor $U(t)$ is written as

$$U = \left(s_1 + \frac{t}{2t_1} \right)^2 . \tag{3.22}$$

In this case, Eqn (3.11) determining the field F is reduced to the wave equation in a free space (z, τ),

$$\frac{\partial^2 F}{\partial z^2} - \frac{1}{v^2} \frac{\partial^2 F}{\partial \tau^2} = 0 \, , \qquad v = \frac{c}{n_0} \, . \tag{3.23}$$

Substitution of (3.22) in (3.8) yields the variable

$$\tau = t \left(1 + \frac{s_1 t}{2t_1} \right)^{-1} . \tag{3.24}$$

Expressing the solution of wave equation (3.23) through an arbitrary function $F\left[(\tau - z/v) t_0^{-1} \right]$ and using (3.8), we can find the electric displacement D_x; thus, for the medium with a decreasing dielectric permeability ($s_1 = -1$), we have

$$D_x = \left(1 - \frac{t}{2t_1} \right) F(u) \, ,$$
$$u = t_0^{-1} \left[t \left(1 - \frac{t}{2t_1} \right)^{-1} - \frac{z}{v} \right] . \tag{3.25}$$

These results, obtained by solving Eqn (3.6) governing the electric displacement D_x, can be found from another equation governing the magnetic field H_y. This equation is derived by eliminating D_x from Maxwell equations (3.4) and (3.5):

$$\frac{\partial^2 H_y}{\partial z^2} - \frac{n_0^2 U^2(t)}{c^2} \frac{\partial^2 H_y}{\partial t^2} = \frac{n_0^2}{c^2} \frac{\partial U^2}{\partial t} \frac{\partial H_y}{\partial t} \, . \tag{3.26}$$

Direct substitution shows that the function H_y in (3.18) is a solution of Eqn (3.26). In Section 4, we show that both these solutions, D_x and H_y, found here for the normal incidence, allow generalization for any arbitrary incidence angles.

Equation (3.26) allows finding a new temporal profile $U(t)$, reducing (3.26) to the form of the wave equation in a free space, Eqn (3.23). This profile is different from (3.22):

$$U^2(t) = \left(1 - \frac{t}{t_m} \right)^{4/3} , \qquad 0 \leqslant t \leqslant t_m = \frac{2t_1}{3} \, . \tag{3.27}$$

The dynamics of an arbitrarily shaped transient traveling in medium (3.27) can be presented by the time-domain solution of Eqn (3.26),

$$H_y = A \left(1 - \frac{t}{t_m} \right)^{-1/3} F(u) \, ,$$
$$u = \frac{t_1}{t_0} \left[\left(1 - \frac{t}{t_m} \right)^{1/3} - 1 + \frac{z}{v t_1} \right] , \tag{3.28}$$

where F is an arbitrary function and A is a normalization constant.

Remarkably, the nonstationarity-induced dispersion does not occur in models (3.22) or (3.27); in particular, the harmonic wave propagation in these media is characterized, unlike (3.15), by the wave vector $q = \omega/v$, i.e., the dispersion factor N in (3.15) is reduced to unity.

We stress again that expressions (3.25) and (3.28) are valid for arbitrary waveforms, including the widely discussed ultrashort single-cycle pulses. These waveforms can be considered the exact analytic solutions in the time-domain optics of nonstationary media.

3.2 Ultrafast variations of reflected fields

To find the time-dependent reflection coefficient R, we must use the continuity conditions for the electric and magnetic field components on the interface $z = 0$ of the nonstationary dielectric. We consider the normal incidence of a monochromatic linearly polarized CW train with frequency ω from the vacuum on the interface $z = 0$. Continuity conditions for the E_x and H_y components, Eqns (3.17) and (3.18), yield the value of the reflection coefficient in this case,

$$R = \frac{N - n_0 U \left(1 + i U_t / (2\omega) \right)}{N + n_0 U \left(1 + i U_t / (2\omega) \right)} \, . \tag{3.29}$$

Formula (3.29) describes the simplest time-dependent generalization of the Fresnel law, visualizing the substantial influence of finite relaxation times t_1 and t_2 on the reflectivity of dielectrics. We use (3.29) to examine some optical effects arising due to the decrease in dielectric permeability, described by the descending branch of curve (3.12). According to this curve (see Fig. 3), the refractive index n is changed from the value $n = n_0$ ($t = 0$) to its minimum value $n = n_0(1 - y^2)$ at the instant $t = t_m$, Eqn (3.14). Assuming that such a change is initiated by fast ionization, we can consider the forthcoming reinstatement of unperturbed values of n as a slow process, determined, e.g., by recombination, its characteristic time being about a nanosecond; this means that during some time after t_m, the graph of $n(t)$ can be approximated by a horizontal line (see Fig. 3). Some salient features of nonstationary reflectivity in the time interval $0 \leqslant t \leqslant t_m$ are listed below:

(A) The reflection coefficient at $t \leqslant 0$ is given by its stationary real value

$$R = \frac{1 - n_0}{1 + n_0}, \qquad \frac{\partial n_0}{\partial t} = 0. \tag{3.30}$$

The beginning of the ionization process provides a discontinuity of the first time derivative of the dielectric permeability:

$$\left.\frac{\partial U^2}{\partial t}\right|_{-0} = 0, \qquad \left.\frac{\partial U^2}{\partial t}\right|_{+0} = -\frac{2s_1}{t_1}. \tag{3.31}$$

This discontinuity results in a jump-like variation of the reflection coefficient from the real value $n = n_0$ to a complex one:

$$\left.R\right|_{+0} = \frac{N - n_0\big(1 - \mathrm{i}s_1/(2\omega t_1)\big)}{N + n_0\big(1 - \mathrm{i}s_1/(2\omega t_1)\big)}. \tag{3.32}$$

The time-variable phase φ in (3.29) also has a discontinuity at $t = 0$.

(B) The smooth variation in the reflection coefficient after its beginning at $t = 0$ is interrupted by another discontinuity at $t = t_{\mathrm{m}}$. At this moment, the dielectric permittivity and its first derivative remain continuous, but the second time derivative U_{tt} in model (3.12) has a discontinuity,

$$\begin{aligned} \left.U_t\right|_{t_{\mathrm{m}}-0} &= \left.U_t\right|_{t_{\mathrm{m}}+0} = 0, \\ \left.U_{tt}\right|_{t_{\mathrm{m}}-0} &= \frac{4n_0(1 - y^2)}{t_2^2}, \\ \left.U_{tt}\right|_{t_{\mathrm{m}}+0} &= 0. \end{aligned} \tag{3.33}$$

This discontinuity leads to a jump-like transition of R from the value $R_{\mathrm{m}} = R(t_{\mathrm{m}})$ to a stationary value R_2:

$$R_{\mathrm{m}} = \frac{N - n_0(1 - y^2)}{N + n_0(1 - y^2)}, \qquad R_2 = \frac{1 - n_0(1 - y^2)}{1 + n_0(1 - y^2)}. \tag{3.34}$$

The graph of the reflection coefficient containing these peculiarities is shown in Fig. 4.
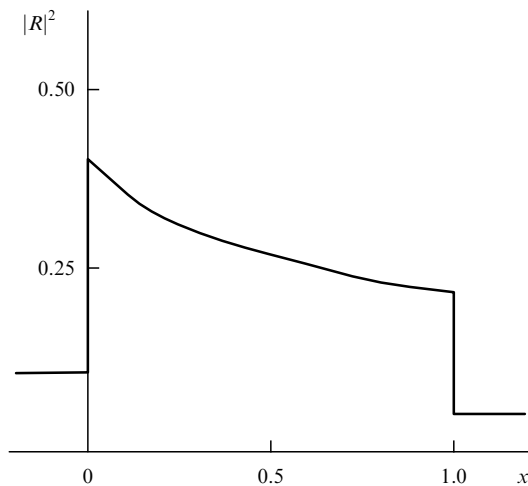
Figure 4. Formation of discontinuities in the time-dependent reflection coefficient with respect to the power $|R|^2$ for the model of dielectric permeability shown in Fig. 3 (branch *2*); $x = t/t_0$.

(C) The distortions of reflected waveforms produced by the aforesaid variations in the reflection coefficient exist during the restricted time interval $0 \leqslant t \leqslant t_{\mathrm{m}}$; during this interval, the initially sinusoidal waveforms can be completely deformed. Thus, in the case where the period of the probing wave $T_{\sim}$ is comparable with the ionization time t_{m}, the reflected CW train of harmonic waves can contain one or a few unharmonic waveforms, located in the interval $0 \leqslant t \leqslant t_{\mathrm{m}}$. This short-lived burst of radiation is characterized by an essential spectral broadening, determined by the time t_{m}. Owing to this effect, the diffraction pattern of the reflected wave includes some weak short-lived sidelobes containing information about the ionization dynamics. The registration of these sidelobes would be a difficult but promising experiment.

It should be emphasized that these reflectivity effects, based on the nonstationarity-induced dispersion, were revealed by means of the exactly solvable model of time-dependent dielectric permeability, Eqn (3.12). The reflection coefficient proves to be dependent on both the current value of $\varepsilon(t)$ and its first and second derivatives. When the influence of these derivatives, described in the expression for reflection coefficient (3.27) by the terms containing $(\omega t_1)^{-1}$ and $(\omega T)^{-2}$, is substantial, we can speak about the dynamical regime of reflectivity. The phase modulation of a reflected wave, described by the time-dependent phase shift $\varphi(t)$ in (3.29), is also inherent in the dynamical regime of reflection.

The opposite case, where these terms are negligible, corresponds to the adiabatic regime; reflection coefficient (3.27) for this regime is written as

$$R = \frac{1 - n_0 U(t)}{1 + n_0 U(t)}. \tag{3.35}$$

The phase modulation of the reflected wave does not arise in this approximation related to nonstationary geometric optics [33]. Finally, when the variation of $U(t)$ is also negligible, expression (3.35) is reduced to the traditional Fresnel formula (3.30), which thus proves to be a limiting case of the more general time-dependent result in (3.29).

It is noteworthy that the model $U(t)$ in (3.12) contains two free parameters: its extremum U_{m} and the time scale t_{m}, $U(t_{\mathrm{m}}) = U_{\mathrm{m}}$. These parameters being fixed, the initial rate of variation of the dielectric permeability, described by the derivative U_t at $t = 0$, is also fixed, see (3.31). However, it is sometimes convenient to keep the given values U_{m} and t_{m} to model the variation of $U(t)$ by means of another value of $\left.U_t\right|_{t=0}$. This can be done in the framework of another exactly solvable model of nonstationary dielectric permeability, presented by the inverse dependence [32]

$$\begin{aligned} \frac{t}{T} = \frac{1}{2}\Bigg\{ &M - \sqrt{U(U - U_{\mathrm{m}})} \\ &+ (1 - M^2)\operatorname{arcosh}\left[\frac{\sqrt{U} - M\sqrt{U - U_{\mathrm{m}}}}{1 - M^2}\right]\Bigg\}. \end{aligned} \tag{3.36}$$

Similarly to (3.12), this model also contains two free parameters, M and T, which are expressed through U_{m} and t_{m}:

$$\begin{aligned} M &= \sqrt{1 - U_{\mathrm{m}}}, \qquad 0 \leqslant M \leqslant 1, \\ \frac{t_{\mathrm{m}}}{T} &= \frac{1}{2}\left[M + (1 - M^2)\operatorname{arcosh}\left(\frac{1}{\sqrt{1 - M^2}}\right)\right]. \end{aligned} \tag{3.37}$$

However, the value of the slope $U_t|_{t=0}$ is different from (3.31):

$$\frac{\partial U}{\partial t}\bigg|_{t=0} = -\frac{2M}{T}\,. \tag{3.38}$$

Until now, we have been speaking about the CW train of monochromatic waves, reshaping due to interaction with the nonstationary dielectric. However, this approach is not convenient for the analysis of the interaction of initially unharmonic broadband single-cycle waveforms with these media. Such pulses are characterized by nonstationary reshaping even in the course of propagation in a free space (see Section 7). The dynamics of some single-cycle waveforms in a plasma-like medium are considered in Ref. [34] in the framework of the time-domain approach.

3.3 Reflectivity of rapidly ionizing plasma
In discussing wave processes in materials with a time-varying dielectric permeability $\varepsilon(t)$, we have not specified the nature of the material. However, the fast and substantial changes in $\varepsilon(t)$ are often attained in plasma ionization; therefore, it makes sense to specially examine the reflection of EM waves from such media, especially because the mathematical basis of this analysis is different from the approach used in Section 3.1.

Reflectivity of ionizing plasma essentially depends on the ionization time. This dependence has been examined numerically (see, e.g., Refs [24, 25] and the references therein); here, we consider some analytic models of the time-dependent density of ionization. We first discuss wave effects stimulated by the growth of the electron density N in a semi-infinite space from the initial value N_1 at the instant $t = 0$ up to its asymptotic value N_m corresponding to the saturation of the ionization process. The time dependence of the plasma density $N(t)$ can be modeled in this case as

$$N(t) = 2N_1 - N_m + \frac{2(N_m - N_1)}{1 + \exp(-t/t_0)}\,, \tag{3.39}$$

where t_0 is the characteristic ionization time. Expressing the field components $\mathbf{E}$ and $\mathbf{H}$ and the electric current $\mathbf{j}$ induced by this field through the vector potential $\mathbf{A}$,

$$\mathbf{E} = -\frac{\partial \mathbf{A}}{\partial t}\,, \qquad \mathbf{H} = \operatorname{rot}\mathbf{A}\,, \tag{3.40}$$

$$\mathbf{j} = -\frac{e^2 N(t)\mathbf{A}}{mc}\,, \tag{3.41}$$

and considering the linearly polarized wave ($\psi = A_x$, $A_y = A_z = 0$), we can write the Maxwell equation for the function ψ:

$$\frac{\partial^2 \psi}{\partial z^2} - \frac{1}{c^2}\frac{\partial^2 \psi}{\partial t^2} = \frac{\psi}{c^2}\left[2\Omega_1^2 - \Omega_m^2 + \frac{2(\Omega_m^2 - \Omega_1^2)}{1 + \exp(-t/t_0)}\right]. \tag{3.42}$$

It is convenient to seek the solution of (3.42) in the form

$$\psi = BF\exp\left[\mathrm{i}(kz - \omega t)\right], \qquad c^2 k^2 = \omega^2 - \Omega_m^2\,. \tag{3.43}$$

Substitution of (3.43) in (3.42) gives an equation for the function F, dependent upon the normalized variable $x = t/t_0$,

$$\frac{\partial^2 F}{\partial x^2} - 2\mathrm{i}p\,\frac{\partial F}{\partial x} - \frac{t_0^2(\Omega_2^2 - \Omega_1^2)\exp(-x)}{1 + \exp(-x)}\,F = 0\,, \qquad p = \omega t_0\,. \tag{3.44}$$

Using the new variable $u = -\exp(-x)$, we can reduce (3.44) to the standard hypergeometric equation (2.31). In so doing, the values of the parameters α, β, and γ in (2.31) are

$$\alpha, \beta = \mathrm{i}t_0\left[\omega \pm \sqrt{\Omega_1^2 - \Omega_m^2 + \omega^2}\right], \qquad \gamma = 1 + 2\mathrm{i}p\,. \tag{3.45}$$

The solution of Eqn (3.44) is represented by the hypergeometric series $F(\alpha, \beta, \gamma, u)$. The convergence condition for this series [35]

$$\mathrm{Re}\,(\alpha + \beta - \gamma) \leqslant 0 \tag{3.46}$$

is satisfied for the values in (3.45): $\alpha + \beta - \gamma = -1$; thus, the vector potential component ψ in (3.43) can be written as

$$A_x = \psi = BF\left[\alpha, \beta, \gamma, -\exp\left(-\frac{t}{t_0}\right)\right]\exp\left[\mathrm{i}(kz - \omega t)\right]. \tag{3.47}$$

Substitution of (3.47) in (3.40) yields the components E_x and H_y; these components, expressed through the hypergeometric function F, are nonsinusoidal. The continuity conditions for E_x and H_y on the interface $z = 0$ give the value of the reflection coefficient:

$$R = \frac{pF - \mathrm{i}uF_u - pFN}{pF - \mathrm{i}uF_u + pFN}\,, \qquad N = \sqrt{1 - \Omega_m^2\omega^{-2}}\,. \tag{3.48}$$

Here, F_u is the derivative of the hypergeometric function; this derivative can be calculated by the formula [35]

$$\frac{\mathrm{d}F(\alpha, \beta, \gamma, u)}{\mathrm{d}u} = \frac{\alpha\beta}{\gamma}\,F(\alpha + 1, \beta + 1, \gamma + 1, u)\,. \tag{3.49}$$

Because the ratio F_u/F is finite, the long-term $(t \gg t_0)$ asymptotic form of the reflection coefficient R in (3.48) is reduced to the stationary limit:

$$\lim R\bigg|_{t \gg t_0} = \frac{1 - N}{1 + N}\,. \tag{3.50}$$

Proceeding in a similar fashion, we can examine the reflectivity of nonstationary plasma in another ionization regime, when the electron density $N(t)$ is growing from the initial value N_1 to its maximum N_m during a finite time t_0. This regime can be described by the model containing three free parameters — the time scale t_0 and the dimensionless quantities Q and G:

$$N(t) = N_1 + G\left[\frac{\cosh^2 Q}{\cosh^2(t/t_0 - Q)} - 1\right]. \tag{3.51}$$

Introducing the characteristic time T determined by the initial growth rate of ionization $N(t)$ (Fig. 5a), we can find the quantities Q and G from the equation following from (3.51):

$$\frac{1}{N}\frac{\mathrm{d}N}{\mathrm{d}t}\bigg|_{t=0} = \frac{2G\tanh Q}{t_0} = \frac{N_m}{T}\,, \tag{3.52}$$

$$Q = \operatorname{artanh}\left(\frac{\sqrt{1 + 4s^2} - 1}{2s}\right), \qquad s = \frac{2T}{t_0}\left(1 - \frac{N_1}{N_m}\right). \tag{3.53}$$

The electron density reaches its maximum value N_m during the time $T_m = t_0\cosh Q$.
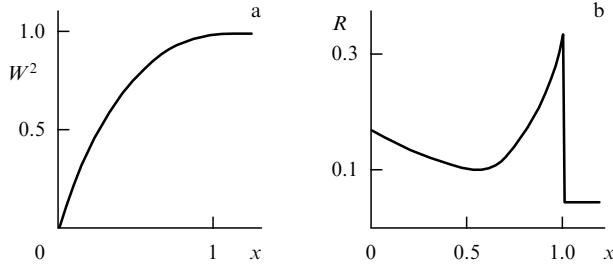
Figure 5. Nonstationary reflectivity of rapidly ionizing plasma: (a) the temporal growth of the normalized ionization density $W = N(t)/N_{\mathrm{m}}$, $N(t)$ is given in (3.51), $x = t/T_0$, $G = 10^{17}$ cm^{-3}, $Q = 3.5$; $W = 1$ when $x \geqslant 1$; (b) the reflection coefficient R for the leading edge of a CW train ($\lambda = 0.8$ μm, $t_0 = 1.25$ fs) for the conditions shown in figure a; when $x \geqslant 1$, the value R remains constant.

The field ψ is described in this case by an equation similar to (3.42):

$$\frac{\partial^2 \psi}{\partial z^2} - \frac{1}{c^2}\frac{\partial^2 \psi}{\partial t^2} = \frac{\psi}{c^2}\left[\Omega_1^2 - \Omega_{\mathrm{m}}^2 + \frac{\Omega_{\mathrm{m}}^2 \cosh^2 Q}{\cosh^2(t/t_0 - Q)}\right]. \quad (3.54)$$

Seeking the solution of (3.54) in the form

$$\psi = BF\exp\left[\mathrm{i}(kz - \omega t)\right], \qquad k^2 c^2 = \omega^2 + \Omega_1^2 - \Omega_{\mathrm{m}}^2, \quad (3.55)$$

we reduce (3.54) to the familiar equation (2.31) for the hypergeometric function $F(u)$ with the parameters α, β, and γ and the variable u given by

$$\alpha, \beta = \frac{1}{2}\left[1 \pm \sqrt{1 + 4(\Omega_{\mathrm{m}}t_0 \cosh Q)^2}\right], \qquad \gamma = 1 + \mathrm{i}p, \quad (3.56)$$

$$u = \frac{1}{2}(1 - \tanh\varphi), \qquad \varphi = \frac{t}{t_0} - Q. \quad (3.57)$$

Because $\mathrm{Re}\,(\alpha + \beta - \gamma) = 0$, the series $F(u)$ converges in accordance with condition (3.46). Continuing this analogy with field (3.47), we can see that the reflection coefficient connected with ionization regime (3.51) is given again by formula (3.48) in which the wavenumber k and the variable u are given in (3.55) and (3.57), respectively.

It is remarkable that for some values of parameters (3.56), the solutions of Eqn (3.54), expressed via the hypergeometric functions F, can be essentially simplified. These functions are known to be reduced to polynomials if the parameters α or β are equal to negative integers. Thus, equating $\beta = -n$, we find the relevant values of the product $(\Omega_{\mathrm{m}}t_0 \cosh Q)^2$ in (3.56),

$$(\Omega_{\mathrm{m}}t_0 \cosh Q)^2 = n(n+1), \qquad n = 1, 2, 3, \ldots. \quad (3.58)$$

With condition (3.58) satisfied, solutions F_n are represented by nth-degree polynomials in the variable u,

$$F_1 = \frac{1 - 2u}{\gamma}, \qquad F_2 = 1 - \frac{6u}{\gamma} + \frac{12u^2}{\gamma(\gamma+1)}. \quad (3.59)$$

Using the definition of φ, we can rewrite these polynomials as

$$F_1 = \frac{\tanh\varphi + \mathrm{i}p}{\gamma},$$

$$\qquad (3.60)$$

$$F_2 = \frac{3\tanh^2\varphi - (1 + p^2) + 3\mathrm{i}p\tanh\varphi}{\gamma(\gamma+1)}.$$

In deriving formulas (3.59) and (3.60), we assumed for simplicity that the probing wave is incident on the plasma interface $z = 0$ at the instant $t = 0$.

Substitution of functions (3.59) in (3.40) and (3.48) yields explicit expressions for the field components E and H and the reflection coefficient R; thus, in the case where $n = 3$, we have

$$R_3 = \frac{-3\tanh\varphi(1 - \tanh^2\varphi)\left[10\tanh\varphi + 2\mathrm{i}p + 3\mathrm{i}p^{-1}(1 - 5\tanh^2\varphi)\right]}{12\tanh\varphi(5\tanh^2\varphi - 4 - p^2) - 2\mathrm{i}p(18\tanh^2\varphi - 7 - p^2) - K},$$

$$K = -9\mathrm{i}p^{-1}(1 - \tanh^2\varphi)(1 - 5\tanh^2\varphi). \quad (3.61)$$

The drastic nonstationary distortions of the reflected waveform, described by the coefficient R_3, are shown in Fig. 5b. This graph illustrates the reflectivity of rapidly ionizing air under normal conditions (the molecular density is given by the Loschmidt number $N = 2.7 \times 10^{19}$ cm^{-3}) for the ionization level 50%, probing wavelength $\lambda = 0.8$ μm, and ionization time $T_{\mathrm{m}} = 1.25\lambda/c$.

We stress some peculiarities of reflectivity in the time interval $0 \leqslant t \leqslant T_{\mathrm{m}}$, shown by this example:

(A) Both amplitude and phase of the complex reflection coefficient are time-dependent, such that the phase shift of R vanishes at the end of the ionization process and the value of R at this moment $t = T_{\mathrm{m}}$ becomes purely real:

$$R\Big|_{T_{\mathrm{m}}} = \frac{3(3 + 2p^2)}{9 + 14p^2 + 2p^4}. \quad (3.62)$$

(B) The discontinuity in the curvature of the temporal profile of ionization $N(t)$ at the instant $t = T_{\mathrm{m}}$ [model (3.51)] results in a jump-like change of the reflection coefficient R from the value in (3.61), dependent on the ionization rate through the parameter p, to the stationary value in (3.62), independent of this parameter. Such a change, in turn, leads to a discontinuity at the trailing edge of the reflected waveform.

(C) Due to the high probing wave frequency ω ($\Omega_{\mathrm{m}}^2 \omega^{-2} = 0.01$), the value of the plasma refraction index is close to unity and, thus, the stationary value of reflection coefficient (3.29) is small: $R = 0.005$. The maximum value of nonstationary reflection coefficient (3.61) is much higher: $R = 0.32$. This temporal variation in R provides the formation of an ultrashort solitary unharmonic reflected pulse from the leading edge of the probing CW train: the half-width of this pulse Δt is much less than the probing wave period $t_\sim$: $\Delta t \approx 0.1 t_\sim$.

Moreover, the reflectivity of rapidly ionizing plasma can open the route to the generation of ultrashort pulses without the 'pedestal', which is important for the creation of a 'plasma mirror' in experiments with the extreme regime of laser–plasma interactions [36–38]. The principle of the 'plasma mirror' is related to focusing a laser beam on a low-reflectivity vacuum, a dielectric interface, such that most of the pedestal is transmitted. As the intensity increases in time, the ionization of the dielectric medium due to multi-photon absorption develops, and the reflection acquires a 'metallic' character. If the electron density exceeds the critical value for the given laser wavelength ($N_{\mathrm{c}} = 1.75 \times 10^{21}$ cm^{-3}, $\lambda = 800$ nm), the reflectivity increases suddenly [39]. The physical fundamentals of a number of effects of electron dynamics in a powerful light field are examined in Ref. [40].

4. Phase effects
in the optics of nonstationary media

The complex reflection coefficients obtained above for different models of media with time-dependent dielectric properties describe the formation of a time-varying phase shift of a reflected wave. This effect was discussed in Section 3 for a simple case — the reflection of normally incident waves. In contrast, a variety of phase phenomena occuring in both the reflection and refraction of waves in the course of oblique propagation are discussed below.

The polarization structure of incident waves is known to provide the difference in reflection of S- and P-polarized waves. Nonstationary generalizations of the classical Fresnel reflection formulas for these waves are obtained in Section 4.1 in the framework of exactly solvable models. The corresponding generalizations of the Snell law, revealing the difference in refraction of S- and P-polarized waves, are also found. The amplitude–phase reshaping of harmonic fields inside the nonstationary dielectric layer is considered in Section 4.2. Similar phenomena in microwave transmission lines with distributed time-dependent parameters are discussed in Section 4.3.

4.1 Polarization phenomena in the reflectivity
of time-varying lossless media

This section is devoted to the analysis of the reflection of waves incident on the immobile interface $z = 0$ of a time-varying dielectric under an arbitrary incidence angle γ. We first consider the model of the time-dependent dielectric permeability $U(t)$ in (3.12) and perform the calculations of the reflection coefficients for S- and P-polarized waves separately. Speaking, for brevity, about S- and P-waves, we can generalize the approach developed above (Section 3.1) for the normal incidence.

(1) S-wave; this wave is characterized by an electric component E_x and magnetic components H_y and H_z. Eliminating the magnetic components from the Maxwell equations,

$$\frac{\partial E_x}{\partial z} = -\frac{1}{c}\frac{\partial H_y}{\partial t}\,, \qquad \frac{\partial E_x}{\partial y} = \frac{1}{c}\frac{\partial H_z}{\partial t}\,,$$
$$\frac{\partial H_z}{\partial y} - \frac{\partial H_y}{\partial z} = \frac{1}{c}\frac{\partial D_x}{\partial t}\,, \tag{4.1}$$

yields an equation similar to Eqn (3.6) for the electric displacement D_x,

$$\frac{\partial^2 D_x}{\partial z^2} + \frac{\partial^2 D_x}{\partial y^2} - \frac{n_0^2 U^2(t)}{c^2}\frac{\partial^2 D_x}{\partial t^2} = 0\,. \tag{4.2}$$

Using the new variable τ in (3.7), we can write the solution of (4.2) as

$$D_x = B\sqrt{U(t)}\,\exp\left[i(k_\perp z + k_\parallel y - \omega\tau)\right], \tag{4.3}$$

where $k_\parallel = \omega c^{-1}\sin\gamma$; the quantities $k_\parallel, k_\perp$, and ω are related by the dispersion equation

$$k_\parallel^2 + k_\perp^2 = \frac{\omega^2}{c^2}\,n_0^2 N^2\,, \qquad N = \sqrt{1 - (\omega T)^{-2}}\,. \tag{4.4}$$

The parameters N and T were determined in (3.13) and (3.15). Omitting the phase factor for simplicity, we obtain the field

components E_x, H_y, and H_z satisfying Maxwell equations (4.1):

$$E_x = \frac{B}{n_0^2 U^{3/2}}\,, \qquad \left\{\begin{array}{c} H_y \\ H_z \end{array}\right\} = \frac{B\big(1 + iU_t/(2\omega)\big)}{n_0 N U^{1/2}}\left\{\begin{array}{c} \cos\gamma \\ -\sin\gamma \end{array}\right\}. \tag{4.5}$$

Here, B is a normalization constant; expressions (4.5) satisfy the condition div $\mathbf{H} = 0$.

To find the reflection coefficient R_s, it is convenient to introduce an angle β such that the components H_y and H_z are written as

$$H_y = H\cos\beta\,, \qquad H_z = -H\sin\beta\,, \qquad H = \sqrt{H_y^2 + H_z^2}\,. \tag{4.6}$$

Using this representation and letting E_i denote the amplitude of the incident wave, we can write the continuity conditions on the interface $z = 0$:

$$E_i(1 + R_s) = Bn_0^{-2}U^{-3/2}\,, \qquad E_i(1 - R_s)\cos\gamma = H\cos\beta\,,$$
$$E_i(1 + R_s)\sin\gamma = H\sin\beta\,. \tag{4.7}$$

Manipulations with conditions (4.7) give the definition of the angle β,

$$\sin\gamma = n_s\sin\beta\,, \qquad n_s = n_0 U N^{-1}\left(1 + \frac{iU_t}{2\omega}\right), \tag{4.8}$$

and the expression for the complex reflection coefficient R_s,

$$R_s = \frac{\cos\gamma - \sqrt{n_s^2 - \sin^2\gamma}}{\cos\gamma + \sqrt{n_s^2 - \sin^2\gamma}}\,. \tag{4.9}$$

Formula (4.8) can be considered the generalized Snell law. The value β in (4.8) is complex: $\beta = \beta_1 + i\beta_2$. This means that equal-phase and equal-amplitude planes are not parallel and hence the normals to these planes form some angle: a similar field structure and a complex refraction angle are known to arise in the wave propagation in an absorbing dielectric [41]. Separation of the real and imaginary parts of (4.8) yields equations for β_1 and β_2:

$$\tan\beta_1 = \frac{1}{gl}\sqrt{\frac{1}{2}\left(-G + \sqrt{G^2 + 4g^2l^2}\right)}\,, \tag{4.10}$$

$$g = \frac{U_t}{2\omega}\,, \qquad l = \frac{N\sin\gamma}{n_0 U}\,, \qquad \tanh\beta_2 = -g\tan\beta_1\,. \tag{4.11}$$

In the case of S-polarization, the quantity G is determined by

$$G = G_s = l^2(g^2 - 1) + (1 + g^2)^2\,. \tag{4.12}$$

(2) P-wave; as opposed to the S-wave, the P-wave field is characterized by a magnetic component H_x and electric components E_y and E_z, related by the equations

$$\frac{\partial H_x}{\partial z} = \frac{1}{c}\frac{\partial D_y}{\partial t}\,, \qquad -\frac{\partial H_x}{\partial y} = \frac{1}{c}\frac{\partial D_z}{\partial t}\,,$$
$$\frac{\partial E_z}{\partial y} - \frac{\partial E_y}{\partial z} = -\frac{1}{c}\frac{\partial H_x}{\partial t}\,. \tag{4.13}$$

Elimination of the electric displacement components D_y and D_z from system (4.13) reduces this system to one equation, similar to Eqn (3.35):

$$\frac{\partial^2 H_x}{\partial z^2} + \frac{\partial^2 H_x}{\partial y^2} - \frac{n_0^2 U^2(t)}{c^2}\frac{\partial^2 H_x}{\partial t^2} = \frac{n_0^2}{c^2}\frac{\partial U^2}{\partial t}\frac{\partial H_x}{\partial t}. \qquad (4.14)$$

Using model (3.12) and the variable τ, we again find the solution of (4.14):

$$H_x = \frac{B}{\sqrt{U}}\left(1 + \frac{\mathrm{i}U_t}{2\omega}\right)\exp\left[\mathrm{i}(k_\perp z + k_\parallel y - \omega\tau)\right]. \qquad (4.15)$$

Proceeding in the fashion used above in the case of an S-wave, we obtain the components E_y and E_z, which satisfy the equation div $\mathbf{E} = 0$. Comparing these H_x, E_y, and E_z components of the P-wave with the E_x, H_y, and H_z components of the S-wave in (4.5), we see that the duality principle, allowing the replacement $\mathbf{E} \rightleftarrows -\mathbf{H}$, $\mathbf{B} \rightleftarrows \mathbf{D}$ in the Maxwell equations, remains valid for nonstationary media.

The continuity conditions for the P-wave yield the nonstationary generalization of the Snell law,

$$\sin\gamma = n_{\mathrm{p}}\sin\beta, \qquad n_{\mathrm{p}} = n_0 N U\left(1 + \frac{\mathrm{i}U_t}{2\omega}\right)^{-1}, \qquad (4.16)$$

and the reflection coefficient R_{p} for P-waves,

$$R_{\mathrm{p}} = \frac{(n_0 U)^2\cos\gamma - \sqrt{n_{\mathrm{p}}^2 - \sin^2\gamma}}{(n_0 U)^2\cos\gamma + \sqrt{n_{\mathrm{p}}^2 - \sin^2\gamma}}. \qquad (4.17)$$

The real part of the complex refraction angle β is then given by Eqn (4.10) due to replacement:

$$G = G_{\mathrm{p}} = l^2(g^2 - 1) + N^4. \qquad (4.18)$$

The imaginary part of β is determined by the expression

$$\tanh\beta_2 = g\tanh\beta_1. \qquad (4.19)$$

The dimensionless parameters l and g were defined in (4.11). It is noteworthy that the complex reflection angles for S- and P-waves are distinguishable, the incidence angle being the same. In the special case where $s_2 = 0$, Eqn (3.13), it can be shown that $N^2 = 1 + g^2$ and, thus, the real parts β_1 for the S- and P-waves coincide; however, even in this case, the imaginary parts β_2 for the S and P waves have opposite signs.

(3) Until now, we have been considering the reflectivity of nonstationary media using the model of time-varying dielectric permeability. In contrast, the reflection – refraction problems for plasmas with rapidly varying ionization were treated in Section 3.3 beyond the scope of this concept. Although the analysis in Section 3.3 was performed for the normal incidence, its generalization to the case of inclined incidence is trivial. Thus, for example, considering the inclined incidence of an S-wave on the interface of plasma with growing ionization (3.51), we can use solution (3.55), (3.56) corresponding to this model, and, by analogy with (4.8), (4.9), derive the time-dependent Snell law

$$\sin\gamma = \frac{\sin\beta}{1 - \mathrm{i}K}, \qquad K = \frac{1}{2p\cosh^2\varphi}\frac{F_u}{F}. \qquad (4.20)$$

The reflection coefficient for this rapidly ionizing area is

$$R_{\mathrm{s}} = \frac{\cos\gamma - \sqrt{(1 - \mathrm{i}K)^2 - \sin^2\gamma}}{\cos\gamma + \sqrt{(1 - \mathrm{i}K)^2 - \sin^2\gamma}}. \qquad (4.21)$$

The attempt to calculate the reflection of P-waves in the framework of this approach faces some analytical difficulties. It is easy to find the components H_x, E_y, and E_z characterizing the polarization structure of a P-wave: thus, the component H_x satisfies the equation similar to (3.54),

$$\frac{\partial^2 H_x}{\partial z^2} + \frac{\partial^2 H_x}{\partial y^2} - \frac{1}{c^2}\frac{\partial^2 H_x}{\partial t^2} = \frac{\Omega^2}{c^2}H_x\left[\frac{\cosh^2 Q}{\cosh^2(t/t_0 - Q)} - 1\right]. \qquad (4.22)$$

The solution of (4.22) was shown in (3.56) to be represented in the form

$$H_x = F(\alpha, \beta, \gamma, u)\exp\left[\mathrm{i}(k_\perp z + k_\parallel y - \omega t)\right],$$

where F is hypergeometric function (3.56). The vector-potential components A_y and A_z are determined by the equation coinciding with (4.22). Substitution of A_y and A_z in (3.40) gives the electric field components E_y and E_z. The problem arises in deriving the reflection coefficient R_{p}, based on the continuity of the electric displacement component D_z. This function, determined in accordance with (4.13) by the expression

$$D_z = c\int\frac{\partial H_x}{\partial z}\,\mathrm{d}t, \qquad (4.23)$$

contains the hypergeometric function $F(\alpha, \beta, \gamma, u)$ in the integrand; this integrand has to be calculated numerically, and then the calculations of β and R_{p} can be completed.

In conclusion, we stress some properties of nonstationary reflection that are common for all the problems discussed:

(A) the complex refraction angles, as well as the effective refractive indices n_{s} in (4.8) and n_{p} in (4.16), were shown to be different for S and P waves. This difference indicates the appearance of a peculiar short-lived birefringence effect for oblique wave propagation in the time-varying isotropic and homogeneous dielectrics. In the case of normal incidence, the difference between S- and P-polarizations vanishes and the power reflection coefficients $|R_{\mathrm{s}}|^2$ and $|R_{\mathrm{p}}|^2$ become equal; it then follows that $R_{\mathrm{s}} = -R_{\mathrm{p}}$ and the values of β_1 and β_2 are reduced to zero: $\beta_1 = \beta_2 = 0$.

(B) Owing to the complex values of n_{s} and n_{p}, the reflection coefficient R_{s} in (4.9) cannot grow to the value $R_{\mathrm{s}} = 1$ corresponding to the total internal reflection; analogously, the coefficient R_{p} in (4.17) cannot fall to the value $R_{\mathrm{p}} = 0$ corresponding to the Brewster effect. Thus, ultrafast variations of the dielectric permeabilities impede the manifestation of these classic phenomena in the optics of time-dependent media.

(C) The time variations of the reflection coefficient can be used for optical measurement of relaxation times of fast phase transitions for some materials. Thus, investigations of nonequilibrium superconductivity have demonstrated an important role of the order parameter in the structure of a superconductor perturbed by photons or injected carriers [42]. On sufficiently short time scales, these perturbations can throw the order parameter (e.g., the energy gap) out of

equilibrium with both the phonon and superconducting systems. The return to equilibrium can be characterized by some relaxation time, which grows in the vicinity of the critical temperature.

Time-resolved optical measurements [43] revealed an abrupt change in the carrier relaxation time when the samples became superconducting. The temperature-dependent investigations of the carrier relaxation time in a high-temperature superconductor film, performed in Ref. [37], were based on the absorption of an ultrashort light pulse by carriers in the film. The subsequent energy relaxation between electrons and photons was monitored by the optical probing of temperature-dependent reflectivity change as a function of the time delay after the excitation pulse. This thermo-optical perturbation decreased the order parameter Δ by destroying the density of superconducting carriers. The relative perturbations of the power reflection coefficient as small as $\delta|R|^2/|R|^2 \approx 1.5 \times 10^{-4}$, measured by means of 80-fs-duration light pulses, vanished during the relaxation time about one or a few picoseconds. Another mechanism of fast thermic variation of a solid's reflectivity is considered in Section 6.

4.2 Unharmonic traveling waves in nonstationary dielectric layers

The accumulation of amplitude–phase distortions in the course of propagation of an EM wave through a time-varying material was shown above to be short-lived; this effect proved to be essential when the relaxation time and the wave period become comparable. The path of such accumulation develops at a distance of only a few wavelengths and, thus, we can speak about some nonstationary layer. To reveal this reshaping of refracted waves, we restrict ourselves to the simple case of the normal incidence of waves on the interface $z = 0$.

Considering the model in (3.12) and the corresponding refracted wave presentation in form (3.15), we draw attention to the phase factor $\exp[i(qz - \omega\tau)]$, expressed through the variable τ in (3.7). In this τ-space, the space–time structure of the field resembles that of a traveling harmonic wave. We emphasize some peculiarities of this structure:

(A) The electric component in (3.17) can be viewed as a nonstationary wave traveling in the (z, τ)-space with a constant phase velocity. However, in the physical space (z, t), the phase velocity varies in time. These variations give rise to a drastic reshaping of waveforms. To determine this reshaping, we must calculate the amplitude of the refracted wave in the plane $z = 0$. This amplitude is known to be expressed through the reflection coefficient R as $E_t = E_0(1 + R)$. Using formula (3.27) for R and (3.17) for the electric component of the refracted field E_t gives the explicit expression for E_t,

$$E_t = \frac{2E_0 N \exp[i(qz - \omega\tau)]}{U\sqrt{U}\,[N + n_0 U(1 + iU_t/(2\omega))]}\,. \tag{4.24}$$

(B) The waveform of the refracted magnetic component H_t in (3.18) is distinguished from E_t by an additional amplitude–phase modulation,

$$H_t = \frac{n_0 U}{N}\left(1 + \frac{iU_t}{2\omega}\right)E_t\,. \tag{4.25}$$

(C) The normalized dielectric permeability U in (3.12) decreases to its minimum value $U_{\rm m} = 1 - y^2$ during the time

$t_{\rm m} = t_2 y$, Eqn (3.14). At the instant $t_{\rm m}$, the derivative U_t is equal to zero and the wavefront position z_0 is determined by the equation

$$qz_0 - \omega\tau(t_{\rm m}) = 0\,. \tag{4.26}$$

The parameter $\tau(t)$ for the descending branch of $U(t)$ under discussion is given in (3.19), with $\tau(t_{\rm m}) > t_{\rm m}$. The leading edge of the wave train is reshaped while traveling through the perturbed area.

Proceeding in a similar fashion, we can examine the propagation of the probing wave through the rapidly ionizing plasma layer created by discharge in gases or laser ionization of solid targets, e.g., bulk quartz [4], described by model (3.51). We consider the transmission of a wave train, whose reflection is depicted in Fig. 5b, using the same values of plasma and wave parameters. In this case, condition (3.58) with $n = 3$ is satisfied and, thus, the refracted field components can be represented by means of (3.61) and (3.62); however, the constant B has to be replaced by the amplitude of the refracted wave E on the interface $z = 0$. We suppose that the plasma layer thickness d exceeds the distance $z_0 = cT_{\rm m}$ traveled by the leading edge during the time of ionization $T_{\rm m} = t_0 Q$ (3.51); therefore, the rest of the path $d - z_0$ is traversed by the wave train in the plasma with a time-independent density. This wave train is partially reflected back on the interface $z = d$. If this plane corresponds to the boundary between ionized and nonionized air, the reflection coefficient R can be found from the boundary condition

$$E_t(1 + R) = H_t(1 - R)\,. \tag{4.27}$$

The refracted waveform traveling in the area $z \geqslant d$ is here determined as $E = E_t(1 + R)$. The leading edge of the refracted waveform is reshaped; being calculated in the framework of model (3.51), such a reshaping yields the formation of a discontinuity at the instant $t = T_{\rm m}$. Comparison of Fig. 5a and Fig. 5b shows that these nonstationary effects are well expressed in the vicinity of the point $t = T_{\rm m}$, where the curvature of the ionization graph (Fig. 5a) is discontinuous.

4.3 Microwave analogies of time-dependent optical effects

It is noteworthy that some of the pioneering research in electromagnetic wave propagation in time-varying media was performed several decades ago not in the optical but in the microwave spectral range. It was shown in Ref. [2] that the velocity of a wave traveling in a microwave transmission line with a distributed inductance L could be modulated due to time variations of the inductance. In view of the remarkable analogy between this microwave and the relevant optical phenomena, it is worth examining such microwave phenomena in detail.

We consider the model of a lossless line characterized by a time-dependent inductance $L = L_0 U^2(t)$. The distribution of the current I and voltage V in this line is known to be described by the set of equations [44]

$$\frac{\partial V}{\partial z} + L_0 U^2 \frac{\partial I}{\partial t} + RI = 0\,, \qquad \frac{\partial I}{\partial z} + C\frac{\partial V}{\partial t} + GV = 0\,, \tag{4.28}$$

where L_0, C, R, and G are the unperturbed line inductance, capacity, resistance, and leakage parameter per unit length; the resistance and leakage currents are neglected below for

simplicity. The parameters L_0 and C are determined, for instance, for the stripline formed by two metal strips and the dielectric substrate between them, according to the formulas [44]:

$$L_0 = 4\pi \times 10^{-7} \frac{d}{b}, \qquad C = \frac{10^{-9}}{36\pi} \varepsilon_r \frac{b}{d}, \qquad (4.29)$$

where ε_r is the effective dielectric permeability of the substrate layer, d and b are its thickness and width, and L_0 and C are expressed here in H m^{-1} and F m^{-1}, respectively. Expressing the current I and voltage V through a generating function ψ,

$$I = -C \frac{\partial \psi}{\partial t}, \qquad V = \frac{\partial \psi}{\partial z}, \qquad (4.30)$$

we can reduce system (4.28) to one equation, similar to Eqn (3.6) discussed above:

$$\frac{\partial^2 \psi}{\partial z^2} - \frac{U^2(t)}{v_0^2} \frac{\partial^2 \psi}{\partial t^2} = 0. \qquad (4.31)$$

Scrutinizing the time variations of the inductance governed by the model $U(t)$ given by (3.12),

$$L = L_0 \left(1 + \frac{s_1 t}{t_1} + \frac{s_2 t^2}{t_2^2}\right)^2 = L_0 U^2(t), \qquad (4.32)$$

we can represent solutions of (4.30) in the form coinciding with (3.16):

$$\psi = B\sqrt{U(t)} \exp\left[\mathrm{i}(qz - \omega\tau)\right], \qquad (4.33)$$

where the variable τ was determined in (3.19) and (3.20). Substitution of the generating function ψ, Eqn (4.33), in (4.30) gives the explicit expressions for the current I and voltage V:

$$I = \mathrm{i}\omega C U^{-1}\left(1 + \frac{\mathrm{i}U_t}{2\omega}\right)\psi,$$
$$V = \mathrm{i}q\psi, \qquad (4.34)$$
$$q = \frac{\omega}{v_0} N, \qquad N^2 = 1 - (\omega T)^{-2}, \qquad Z = \sqrt{\frac{C}{L_0}}.$$

Here, Z is known to be the impedance of the line with constant values of L_0 and C. Considering the quantity $v_0/U(t)$ in (4.31) as the time-modulated velocity of wave propagation, we can interpret the formation of unharmonic current and voltage waves (4.34) as the result of this velocity modulation. The finite relaxation times of inductance variations determine the frequency dispersion of this transmission line. Expressions (4.30) for the instantaneous voltage and current resemble expressions (3.17) and (3.18) for unharmonic electric and magnetic fields. Using the Kirchhoff rules for voltage and current instead of continuity conditions for the components of the EM field allows investigating the reflection of waves in the homogeneous transmission line due to switching of time-varying inductance at some segment of this line. Thus, the reflection coefficient R_c with respect to the current, derived from Eqn (4.34), is

$$R_c = \frac{Z_0\left(1 + \mathrm{i}U_t/(2\omega)\right) - NUZ}{Z_0\left(1 + \mathrm{i}U_t/(2\omega)\right) + NUZ}. \qquad (4.35)$$

The value R_c is complex, the line being lossless; the imaginary part of R_c is linked with the time-varying inductance.

The effect of velocity modulation can be used for the optimization of the parameters of the tunable delay line. Thus, we suppose that the inductance $L(t)$ in (4.31) grows ($s_1 = 1$, $s_2 = -1$) from the initial value L_0 up to its maximum L_m during the time T. We then find the distance l passed by the zero-crossing point, which traverses the input of the line at the instant $t = 0$.

The condition $ql - \omega\tau = 0$, Eqn (4.33), yields the distance l; calculating the value of $\tau(t)$ from (3.20), we obtain

$$l = \frac{v_0 T}{2y\sqrt{1 + y^2}} \ln\left(\frac{y_+}{y_-}\right), \qquad y_\pm = \sqrt{1 + y^2} \pm y. \qquad (4.36)$$

The parameter $y = t_2/(2t_1)$ is expressed through the quantities L_0 and L_m as

$$y = \sqrt{\sqrt{\frac{L_m}{L_0}} - 1}. \qquad (4.37)$$

On the other hand, the same point on the wave envelope, while traveling in the line with a constant inductance L_0, passes the distance $l_0 = v_0 T < l$; hence, in the case where $y = 0.5$, we have $l = 0.85 l_0$. Therefore, the nonstationary inductance results in a deceleration of the wave during the transition time.

In concluding this section, it is worth mentioning the adiabatic limit of the expressions derived above. This limit corresponds to the case of a 'slow' modulation of the dielectric permeability, with $U_t/\omega \to 0$, $U_{tt}/\omega^2 \to 0$, $N \to 1$. In this limit, the distinguished expressions for the effective refraction indices n_s in (4.8) and n_p in (4.16) degenerate to the coinciding ones,

$$n_s = n_p = n_0 U(t). \qquad (4.38)$$

Substitution of (4.35) in Fresnel laws (4.9) and (4.17) gives the adiabatic values of the reflection coefficients R_s and R_p for S- and P-polarized waves. We also note the peculiar case where $N = 1$, although both U_t and U_{tt} retain finite values. This situation, occuring in model (3.12) with $s_2 = 1$, $y = 1$, was presented above by dependence (3.22).

5. Electromagnetic fields in variable spatiotemporal structures

Until now, the analysis of problems of EM wave propagation in nonstationary media was restricted by assumptions about the spatially homogeneous temporal variations of these media. However, there is a multitude of problems where both temporal and spatial variations of dielectric parameters affecting the wave propagation must be taken into account. The simplest example of such effects, connected with the motion of an ionization front separating gas bulks with different dielectric permeabilities, was mentioned briefly in Section 3. The more complicated effect of reflectivity of a moving ionization front was observed in the course of ultrafast ionization of solid targets, e.g., quartz [4], resulting in the formation of the so-called 'plasma mirror'. The oscillations of this mirror, excited by alternating pressures of a pumping beam, provide the phase modulation phenomena in a reflected wave, including, in particular, generation of harmonics.

The optical effects of traveling perturbations, forming smoothly varying spatiotemporal structures, are usually examined by means of computer simulation; a detailed description of such procedures is given, e.g., in Ref. [45]. The development of the analytic theory of such effects remains a hot topic in the electrodynamics of continuous media. By contrast, the analytic approach in the theory of wave interaction with immobile spatiotemporal structures is elaborated somewhat better. The mathematical scheme of this theory is based on the representation of the dielectric permeability of the medium as a product of two functions: one dependent only on spatial coordinates and the other dependent only on time:

$$\varepsilon(\mathbf{r}, t) = n_0^2 W^2(\mathbf{r}) U^2(t). \tag{5.1}$$

Some problems that can be investigated in the framework of this approach are considered below for nonstationary EM waves traveling in a transmission line (Section 5.1), standing in a cavity (Section 5.2), and traversing a heterogeneous layer (Section 5.3). Despite the differences in the physical statement of these problems, they are unified mathematically by the factored representations of the spatiotemporal dependences of their dielectric parameters.

5.1 Transition regimes in a transmission line with spatially distributed parameters

Unlike the transition regime in a line with a time-dependent inductance and constant capacity examined above (Section 4.3), we focus attention here on a more complicated system whose parameters vary in both time and space. To simplify the analysis, we again consider the time-dependent inductance $L(t)$ in form (4.32), assuming that the capacity per unit length is spatially distributed as

$$C(z) = C_0 W^2(z), \qquad W(z) = \left(1 + \frac{s_1 z}{L_1} + \frac{s_2 z^2}{L_2^2}\right)^{-1}. \tag{5.2}$$

The equation for the generating function ψ in (4.30), describing the transmission line under discussion, can be derived by analogy with (4.31), with distribution (5.2) taken into account:

$$\frac{\partial^2 \psi}{\partial z^2} - \frac{W^2(z)}{v_0^2 U^2(t)} \frac{\partial^2 \psi}{\partial \theta^2} = 0, \qquad \theta = \int_0^t \frac{\mathrm{d}t_1}{U^2(t_1)}. \tag{5.3}$$

The forthcoming analysis can be viewed as a generalization of Eqn (4.31) and its solution (4.33). We introduce a new function F and variables η [46] and τ_1:

$$F = \frac{\psi}{\sqrt{W(z)U(t)}}, \qquad \eta = \int_0^z W(z')\,\mathrm{d}z', \qquad \tau_1 = \int_0^\theta \frac{\mathrm{d}\theta'}{U(\theta')}. \tag{5.4}$$

Considering models (4.32) and (5.2) and imposing the additional condition $U^2(t)U^2(\theta) = 1$, we obtain an equation for the function F:

$$\frac{\partial^2 F}{\partial \eta^2} - \frac{1}{v_0^2} \frac{\partial^2 F}{\partial \tau_1^2} = \frac{D^2 F}{v_0^2}, \qquad D^2 = T^{-2} - (pv_0)^2. \tag{5.5}$$

The simplest example of a pair of functions related by the above condition $U^2(t)U^2(\theta) = 1$ is

$$U(t) = 1 + \frac{t}{t_1}, \qquad U(\theta) = \left(1 + \frac{\theta}{t_1}\right)^{-1}.$$

The characteristic time T for model (4.32) was defined in (3.13) and the parameter p^2 is connected with the heterogeneity profile in (5.2):

$$p^2 = \frac{s_2}{L_2^2} - \frac{s_1^2}{4L_1^2}. \tag{5.6}$$

The parameter D^2 in (5.5) characterizes the simultaneous influence of heterogeneity- and nonstationarity-induced dispersion. The solution of Eqn (5.5) can be represented as a harmonic wave in the (η, τ_1)-space. Substitution of this solution in (5.4) yields the generating function for the transmission line,

$$\psi = \sqrt{W(z)U(t)} \exp\left[\mathrm{i}(q\eta - \omega\tau_1)\right], \tag{5.7}$$

$$q = \frac{\omega}{v_0}N, \qquad N^2 = 1 - \frac{D^2}{\omega^2}. \tag{5.8}$$

The result in (5.7) describes the multitude of transition regimes in the transmission line with a nonuniformly distributed capacity. For example, we consider the spatial variation of capacity distributed according to (5.2) along a line segment of length l; the capacity C decreases from C_0 to the value C_m at the point $z = 0.5l$ and then increases to the value C_0 at the point $z = l$. Substitution of (5.2) in (5.4) gives the variable $\eta(z)$ in this case,

$$\eta(z) = \frac{l}{2Y\sqrt{1-Y^2}} \arctan\left(\frac{2Y\sqrt{1-Y^2}\,z/l}{l - 2Y^2 z/l}\right), \tag{5.9}$$

$$Y = \sqrt{1 - \sqrt{\frac{C_0}{C_m}}}. \tag{5.10}$$

The length l of the segment corresponds to the value $\eta_0 = \eta(l)$,

$$\eta_0 = \frac{l}{2Y\sqrt{1-Y^2}} \arctan\left(\frac{2Y\sqrt{1-Y^2}}{1 - 2Y^2}\right). \tag{5.11}$$

It makes sense to isolate the special case $D = 0$, where the contributions to dispersion of the transmission line produced by heterogeneous capacity and time-dependent inductance are mutually compensated. A similar situation was mentioned in Section 3.1 for a special type of time variation of refractive index (3.22), the medium being homogeneous. However, the interplay of spatial and temporal variations of the wave velocity $v(z, t) = v_0/\big(U(t)W(z)\big)$ was shown to provide a flexible choice of parameters, resulting in a peculiar regime of propagation $D = 0$ in a transmission line. In this case, equation (5.5) is reduced to the form

$$\frac{\partial^2 F}{\partial \eta^2} - \frac{1}{v_0^2} \frac{\partial^2 F}{\partial \tau^2} = 0. \tag{5.12}$$

Equation (5.12) describes the distortionless propagation of an arbitrarily shaped pulse $F(\tau_1 - \eta/v_0)$ in the (τ_1, η)-space; the dependences $\eta = \eta(z)$ and $\tau_1 = \tau_1(t)$ determine the controlled reshaping of this pulse in the physical space (z, t).

It is remarkable that the mathematical formalism developed above proves to be useful for the analysis of another wave problem, propagation of Alfven waves through heterogeneous time-varying plasma. We consider a circularly polarized Alfven wave that travels along the external

homogeneous magnetic field H_0 (z-direction). We suppose that the plasma density N is coordinate-dependent and the magnetic field varies in time:

$$N = N_0 W^2(z), \qquad H = H_0 U^2(t). \tag{5.13}$$

The dimensionless functions $W(z)$ and $U(t)$ satisfy the conditions

$$W\Big|_{z=0} = 1, \qquad U\Big|_{t=0} = 1. \tag{5.14}$$

The coupled transverse perturbations of the plasma velocity v and magnetic field H induced by the Alfven wave are governed by the equations of magnetic hydrodynamics [47]:

$$\frac{\partial H_\perp}{\partial t} = H_0 U(t)\, \frac{\partial v_\perp}{\partial z}, \tag{5.15}$$

$$\frac{\partial v_\perp}{\partial t} = \frac{H_0 U(t)}{4\pi N_0 W^2(z)}\, \frac{\partial H_\perp}{\partial z}. \tag{5.16}$$

Introducing the normalized variables

$$v = \frac{v_\perp}{v_{\mathrm A}}, \qquad b = \frac{H_\perp}{H_0}, \tag{5.17}$$

where $v_{\mathrm A} = H_0/\sqrt{4\pi N_0}$ is the Alfven velocity, and choosing the generating function $\psi(z,t)$ such that

$$b = \frac{\partial \psi}{\partial z}, \qquad v = \frac{1}{v_{\mathrm A} U(t)}\, \frac{\partial \psi}{\partial t}, \tag{5.18}$$

we reduce system (5.15), (5.16) to one equation [48]:

$$\frac{\partial^2 \psi}{\partial z^2} - \frac{W^2(z)}{v_{\mathrm A}^2 U^2(t)}\left(\frac{\partial^2 \psi}{\partial t^2} - \frac{U_t}{U}\frac{\partial \psi}{\partial t}\right) = 0. \tag{5.19}$$

Using the new variable

$$\tau = \int_0^t U(t')\,\mathrm{d}t' \tag{5.20}$$

permits us to eliminate the unknown time variation of the magnetic field $U(t)$ from Eqn (5.19):

$$\frac{\partial^2 \psi}{\partial z^2} - \frac{W^2(z)}{v_{\mathrm A}^2}\frac{\partial^2 \psi}{\partial \tau^2} = 0. \tag{5.21}$$

It is worth stressing the similarity of Eqns (5.21) and (5.3). Again considering the profile of plasma density in (5.2) and continuing this analogy, we can represent the solution of (5.21) in the form

$$\psi = \sqrt{W(z)}\, \exp\left[\mathrm{i}(q\eta - \omega\tau)\right]. \tag{5.22}$$

The variable η is defined in (5.4) and the wavenumber q depends on the heterogeneity parameter p in (5.6),

$$q = \frac{\omega}{v_{\mathrm A}}\sqrt{1 - \frac{(p v_{\mathrm A})^2}{\omega^2}}. \tag{5.23}$$

Substitution of (5.22) in (5.18) gives the explicit expressions for the plasma velocity $v_\perp$ and transverse magnetic component $H_\perp$ in the field of the Alfven wave traversing a heterogeneous plasma layer. Unlike these waves in homogeneous magnetoplasma, the Alfven waves under discussion

are characterized by strong heterogeneity-induced dispersion.

Because solution (5.22) is independent of the specific model of temporal profile $U(t)$, this solution seems to be rather general. In particular, the case where $q = 0$, Eqn (5.23), corresponds to the propagation of an arbitrarily shaped Alfven pulse in plasma (5.13) along a time-varying magnetic field, its temporal variations being also arbitrary. This analysis may be interesting for problems of both gaseous [49] and semiconductor [50] plasmas.

5.2 Time-domain optics
of nonstationary heterogeneous layers
Along with the model of spatiotemporal variations of the dielectric permeability $\varepsilon(z,t)$ used in (5.1), it is worth discussing another factored representation of $\varepsilon(z,t)$ in the form

$$\varepsilon(z,t) = n_0^2\left[1 - \frac{t}{TF(z)}\right]^2, \tag{5.24}$$

where T is some time scale and $F(z)$ is an arbitrary function. Model (5.24) can be used for the analysis of delay time characterizing the propagation of an EM pulse through a time-varying heterogeneous dielectric layer.

To calculate these delay times, we find the characteristic curves for wave equation (5.2) with the dielectric function $\varepsilon(z,t)$ given by (5.24). The equation governing such a curve with a positive slope in the (z,t) plane is

$$\frac{\mathrm{d}t}{\mathrm{d}z} = \frac{1}{v_0}\left[1 - \frac{t}{TF(z)}\right]. \tag{5.25}$$

This equation is solvable after multiplication with an integrating factor $\theta(z)$ [51]:

$$v_0\left[\frac{\mathrm{d}(t\theta)}{\mathrm{d}z} - t\frac{\mathrm{d}\theta}{\mathrm{d}z}\right] = \theta - \frac{t\theta}{TF(z)}. \tag{5.26}$$

Equalizing the terms in (5.26) containing the factor t, we find the function

$$\theta = \exp\left(\frac{1}{v_0 T}\int_0^z \frac{\mathrm{d}z'}{F(z')}\right). \tag{5.27}$$

The remaining terms in (5.26) determine the characteristic curve passing through the point $(0, t_0)$ in the plane (z,t):

$$v_0(t\theta - t_0) = \int_0^z \theta(z')\,\mathrm{d}z'. \tag{5.28}$$

It was emphasized above that the equation of characteristic line (5.28) is valid for an arbitrary spatial profile of the dielectric permeability $F(z)$ inside a layer. To give an example of an analytic calculation of travel time, we consider the simplest permeability profile $F(z) = 1 + z/L$, where L is some spatial heterogeneity scale. Using Eqns (5.27) and (5.28) gives the explicit expression for the time of travel $t_\sim$ through a layer with thickness d:

$$\frac{t_\sim}{T} = \frac{t_0}{T\theta(d)} + \frac{q}{q+1}\left[1 + \frac{d}{L} - \frac{1}{\theta(d)}\right], \tag{5.29}$$

$$\theta(d) = \left(1 + \frac{d}{L}\right)^q, \qquad q = \frac{L}{v_0 T}.$$

The result in (5.29) is physically acceptable provided $t_\sim < T$ and $t_0 < T$.

It is worth checking formula (5.29) and finding its limit related to the nonstationary layer with vanishing spatial heterogeneity ($L \to \infty$, $F \to 1$) and the same thickness d. In this case, the limit of the function $\theta(d)$ is

$$\lim \theta(d)\Big|_{L \to \infty} = \exp(a), \qquad a = \frac{d}{v_0 T}, \qquad (5.30)$$

and Eqn (5.29) yields

$$\frac{t_\sim}{T} = 1 + \left(\frac{t_0}{T} - 1\right) \exp(-a). \qquad (5.31)$$

On the other hand, one can suppose from the very beginning that the layer is spatially homogeneous and, thus, model (5.24) is reduced to $\varepsilon = n_0^2(1 - t/T)^2$. The calculation of the propagation time $t_\sim$ by means of a wave equation with this model of $\varepsilon(t)$ gives the same result (5.31).

5.3 Generation of photons in time-dependent dielectrics

It was shown above that the interaction of traveling EM waves with a nonstationary dielectric results in spectral broadening of the wave field; one can speak about the generation of new harmonics. A similar effect is examined below for the eigenmodes in a cavity with time-varying eigenfrequencies $\varepsilon(t)$. These variations can be produced, for instance, due to a nonlinear modulation of the dielectric permeability of the medium in a cavity by some external pumping wave [52]. Another possibility for producing such variations is connected with using a cavity with movable perfectly reflecting walls [53]. An interesting situation involving the moving mirror in a cavity is a resonant perturbation, arising when the mirror oscillates periodically with the period of some cavity's eigenfrequency. Owing to this resonance, the field inside the cavity and the moving mirror become strongly coupled. In particular, the generation of THz eigenmodes can be expected in a microwave cavity due to mirror oscillations with hypersound frequencies if the amplitudes of these oscillations are sufficiently large [54].

We consider the mechanism of eigenmode generation using the factored representation of the dielectric permeability in (5.1). The vector potential $\mathbf{A}$ and electric displacement $\mathbf{D}$ for the nth mode can also be sought in a factored form:

$$\mathbf{A}(\mathbf{r}, t) = \mathbf{g}(\mathbf{r})\, u(t), \qquad \mathbf{D}(\mathbf{r}, t) = \varepsilon(\mathbf{r})\, \mathbf{g}(\mathbf{r})\, v(t). \qquad (5.32)$$

We suppose that the function $g(r)$ satisfies the equation [12]

$$\text{rot rot } \mathbf{g} = \frac{\omega_n^2}{c^2}\, \varepsilon(\mathbf{r})\, \mathbf{g}, \qquad (5.33)$$

where ω_n is the eigenfrequency for the nth mode, defined, for example, for the rectangular cavity in (2.1). The solutions of Eqn (5.33) can be chosen to be real vector functions satisfying the orthogonality conditions

$$\int \varepsilon(\mathbf{r})\, \mathbf{g}_n(\mathbf{r})\, \mathbf{g}_m(\mathbf{r})\, d\mathbf{r} = \delta_{nm}. \qquad (5.34)$$

Expressing the field components $\mathbf{E}$ and $\mathbf{H}$ via the vector potential $\mathbf{A}$ by means of (3.40) and using Maxwell equations,

we obtain ordinary differential equations for time-dependent factors of the vector potential $\mathbf{A}$ and electric displacement $\mathbf{D}$:

$$\frac{du}{dt} = -\frac{cv}{u^2(t)}, \qquad \frac{dv}{dt} = \frac{u\omega_n^2}{c}. \qquad (5.35)$$

System (5.35) can be replaced by one second-order differential equation,

$$\frac{d^2 v}{dt^2} + \frac{\omega_n^2 v}{u^2(t)} = 0. \qquad (5.36)$$

Equation (5.36) resembles the equation of motion of the oscillator with a time-dependent frequency. Some of such oscillators are well known in classical [55] and quantum [18] mechanics. As the first example, we consider the case of parametric excitation, where the properties of a medium oscillate harmonically with the frequency Ω equal to the doubled frequency of the nth eigenmode: $\Omega = 2\omega_n$. This can be achieved, for example, by means of a change in the density of the medium due to the action of a powerful external monochromatic pumping wave, running in the transverse direction. Considering the factor $u^{-2}(t)$ in (5.36) represented as a sum,

$$u^{-2}(t) = 1 + \varkappa \cos(2\omega_n t), \qquad |\varkappa| \ll 1, \qquad (5.37)$$

and using the theory of parametric generation [55], we can seek the solution of (5.36) in the form

$$v(t) = \mu(t) \exp(-i\omega_n t) + v(t) \exp(i\omega_n t), \qquad (5.38)$$

with slowly varying time-dependent amplitudes $\mu(t)$ and $v(t)$. Substituting (5.38) and (5.37) in (5.36), neglecting the second-order derivatives of slowly varying amplitudes, and averaging over fast oscillations with the frequency ω_n, we arrive at the pair of equations

$$\frac{d\mu}{dt} = -\frac{i\omega_n \varkappa v}{4}, \qquad \frac{dv}{dt} = \frac{i\omega_n \varkappa \mu}{4}, \qquad (5.39)$$

whose solutions are

$$\mu(t) = \cosh\left(\frac{\omega_n \varkappa t}{4}\right), \qquad v(t) = i \sinh\left(\frac{\omega_n \varkappa t}{4}\right). \qquad (5.40)$$

If the nth eigenmode was not excited at the initial instant $t = 0$, the amount of photons related to this mode at some moment t is given by [12]

$$|v(t)|^2 = \sinh^2\left(\frac{\omega_n \varkappa t}{4}\right). \qquad (5.41)$$

For large values of the parameter $\omega_n \varkappa t \gg 4$, this amount increases exponentially with time. In the real case of a cavity with a finite Q-factor, formula (5.41) is valid provided time t is less than the relaxation time $t_c = Q/\omega_n$. Even in the case of the Q-factor as large as 10^7 and the coupling parameter $\varkappa \sim 10^{-4} - 10^{-5}$, the number of photons in (5.41) is difficult to register in the experiment.

The modification of this vibrating cavity scheme is connected with the accelerated motion of the dielectric when, for example, the cavity formed by two parallel perfectly reflecting planes remains immobile and the dielec-

tric slab initially located between these planes is rapidly removed. Calculations [53] show that such a removal is accompanied by generation of photons.

6. Electrodynamics of media with time-dependent dissipation

In considering the wave effects in media with rapidly varying dielectric parameters, dissipation phenomena have been ignored. It was assumed that the dissipative distortions of an EM field developed more slowly than the nonstationarity-induced reshaping processes. Under this assumption, some time-independent absorption can be easily considered, for example, in the framework of the model $U(t)$ in (3.12) with $U(t)$ replaced with the sum $U(t) + Y$, where $Y = \mathrm{const}$. As distinguished from this, we now examine some wave processes characterized by time-dependent resistance or absorption.

One of the first investigated processes of this kind was connected with the dynamics of lightning. The time-dependent resistance $R(t)$ per meter in the lightning channel, growing due to ionization of the air, was modeled in Ref. [56] as $R(t) \sim \exp{(t/t_0)} - 1$ with $t_0 \sim$ μs. Similar phenomena on the ns scale were discussed for spark discharges in high-voltage laboratory devices [57].

Another display of nonstationary conductivity was connected with cross-modulation of radiowaves in the ionospheric collisional plasma [47]. The heating of electrons by a powerful wave results in a periodic modulation of the electron temperature and, respectively, the frequency of temperature-dependent electron-neutral collisions. These variations yield temporal changes in the plasma conductivity and, in this manner, the modulation of absorption of another probing wave traversing the perturbed region. The characteristic times of the modulation of absorption due to this thermic effect are known to be much longer then the time of collisions between electrons and heavy particles [47].

The temporal variations in dissipation in optical systems can develop faster by far. These effects are illustrated below by optical filters with saturating absorption (Section 6.1) and the tuning of reflectivity of some semiconductors due to thermic variation in their absorption (Section 6.2). Some problems related to the telegraph equation with a time-varying conductivity are discussed in Section 6.3.

6.1 Saturation of absorption

The reflection–refraction processes in a layer with time-varying absorption attract attention as the basis for saturating absorbing wave filters. Such filters can be examined due to appropriate generalization of the model in (3.12), $\varepsilon(t) = n_0^2 U_1^2(t)$:

$$U_1(t) = \begin{cases} 1 + \mathrm{i}\rho_0 \left(1 \mp \dfrac{t}{T_1} \pm \dfrac{t^2}{T_2^2} \right), & 0 \leqslant t \leqslant t_\mathrm{m}, \\ 1 + \mathrm{i}\rho_\mathrm{m}, \quad \rho_\mathrm{m} = \rho_0(1 \mp y^2), & t \geqslant t_\mathrm{m}, \quad y = \dfrac{T_2}{2T_1}. \end{cases}$$
(6.1)

The imaginary part of the normalized complex refractive index $U_1(t)$ varies from the initial value to its extremal value during the saturation time t_m. This saturation of absorption can be considered a result of the 'pump–probe' interaction, when the nonlinear absorption of the pump wave results in the transition of molecules to a new level responsible for attenuation of the probing wave. The time t_m, dependent on

the power of the pump wave and the transition kinetics, may be as short as several picoseconds or may become even comparable with the rise time of the pumping pulse. To stress the effects caused by the saturation of absorption, the real part of $U_1(t)$ is supposed to remain constant.

It is easy to modify the solution of Eqn (3.6) in accordance with the new representation for U_1 in (6.1). Substitution of (6.1) in (3.3) gives the wavenumber q; thus, in the case of increasing absorption, the value of q is

$$q = \frac{\omega n_0}{c} N,$$

$$N = \sqrt{1 - \frac{\rho_0^2}{4\omega^2 T_1^2} + \mathrm{i}\rho_0 \left(1 - \frac{1}{\omega^2 T_2^2} \right)}.$$
(6.2)

The solution of Eqn (3.6) in the time interval $0 \leqslant t \leqslant t_\mathrm{m}$ can be written as traveling wave (3.16),

$$\psi = \sqrt{U_1} \exp{\left[\mathrm{i}(qz - \omega\tau) \right]},$$

dependent on the wavenumber q in (6.2) and the variable τ:

$$\frac{\tau}{T_2} = -\frac{\mathrm{i}}{2S\sqrt{\rho_0}} \ln \left(\frac{1 + t/t_-}{1 - t/t_+} \right), \qquad t_\pm = ST_2 \pm t_\mathrm{m},$$

$$S = \sqrt{\rho_0(1 + y^2) - 1}, \qquad y = \frac{T_2}{2T_1}.$$
(6.3)

It is worth mentioning some peculiarities of this traveling wave:

(A) The wave propagation is characterized by dispersion described by the complex parameter N in (6.2) and dependent on the relaxation times of variable absorption.

(B) The value $\mathrm{Im}\, N$ determines the spatial scale of the exponential decay of the wave field. In the case of decreasing absorption, the imaginary term in the expression for N is replaced by $\mathrm{i}\rho_0 \left[1 - (\omega T_2)^{-2} \right]$. Thus, due to the dispersion produced by decreasing absorption, this decay vanishes for the frequency $\omega = T_2^{-1}$; the value of N in this case is real: $N = \sqrt{1 - y^2}$.

(C) In the limiting case of vanishing absorption, the wavenumber q and variable τ tend to the values $q = \omega n_0/c$ and $\tau = t$ corresponding to the traveling wave in a stationary medium.

Proceeding according to the technique developed in Section 3.1 for a conservative medium, we find the reflection and transmission coefficients for the medium discussed. The saturation of absorption provides the change of the reflection coefficient R, from the initial value R_1 to the value R_2, for example, in the case of normal incidence:

$$R_1 = \frac{1 - n_0(1 + \mathrm{i}\rho_0)}{1 + n_0(1 + \mathrm{i}\rho_0)}, \qquad R_2 = \frac{1 - n_0(a + \mathrm{i}b)}{1 + n_0(a + \mathrm{i}b)},$$

$$a, b = \sqrt{\sqrt{1 + \rho_0^2(1 + y^2)^2} \pm 1}.$$
(6.4)

It makes no sense here to derive the complicated expressions for the modulus $|R_2|^2$ and phase φ_2; the computer calculation of these parameters is easily programmable.

Depending on the saturated value of absorption parameter (6.1), the saturation can result in both an increase and a decrease in reflectivity. Thus, considering the medium with

$n_0 = 1.7$ and $\rho_0 = 1$, we can find from (6.4) that the power reflection coefficient $|R_1|^2$ at the time before the beginning of the saturation process is $|R_1|^2 = 0.33$. The saturation with $y = 1$ results in a decrease in reflection,

$$|R_2|^2 = 0.27 < |R_1|^2 \,,$$

while in the case where $\rho_m = 25\rho_0$ ($y = 4.9$), the reflection coefficient grows:

$$|R_2|^2 = 0.72 > |R_1|^2 \,.$$

The regime of attenuated transmission (the transmission factor $|T_2|^2 = 1 - |R_2|^2 = 0.28$ decreases compared to the initial value $|T_1|^2 = 0.67$) indicates the effect of saturated absorption. This nonmonotonic variation of $|R_2|^2$ accompanying the growth of absorption can become even more complicated with the time variations of the real part of $U_1(t)$ taken into account. The same analysis remains valid in the case of decreasing absorption and in the case of an amplifying medium.

6.2 Thermic modulation of a semiconductor reflectivity
This section is devoted to the thermic tuning of reflectivity of some semiconductors with free carriers belonging to the $A^{III}B^V$ group, e.g., InP, InSb, and GaAs. The well-known method of such tuning is based on the modulation of the free-carrier density in a semiconductor plasma produced by powerful laser radiation and providing the transition of electrons to the conductivity zone. In contrast, the thermic modulation of conductivity connected with Joule heating of carriers in the collisional plasma of semiconductors does not need the generation of any new carriers because it is based on the change in frequency of their collisions; the energy expenditure in such a process is much less.

The perturbations of the semiconductor's dielectric parameters, caused by thermic variations in the frequency of carrier collisions, are usually small. However, these perturbations can be essentially strengthened due to a special choice of parameters of the cross-modulation process, when the plasma frequency Ω_p, the reflecting wave frequency ω, and the frequency of collisions v satisfy the condition

$$\Omega_p \approx \omega \approx v \,. \tag{6.5}$$

With this condition satisfied, both real and imaginary parts of the dielectric permeability,

$$\mathrm{Re}\,\varepsilon = \varepsilon_L \left[1 - \frac{\Omega_p^2}{\omega^2 + v^2(T_e)} \right] \,,$$
$$\mathrm{Im}\,\varepsilon = \frac{v(T_e)\varepsilon_L \Omega_p^2}{\omega[\omega^2 + v^2(T_e)]} \,, \tag{6.6}$$

can be deeply modulated owing to thermic variations in $v(T_e)$; here, T_e is the carrier's temperature, ε_L is the static value of the dielectric permeability, and $\Omega_p^2 = 4\pi e^2 N/(m^*\varepsilon_L)$; for simplicity, we consider only one type of carrier, e.g., electrons with the effective mass m^* and density N. The reflection coefficient for the waves incident normal to the interface of medium (6.6) can be written as

$$R = \frac{1-n}{1+n}\,, \qquad n = \sqrt{\mathrm{Re}\,\varepsilon + \mathrm{i}\,\mathrm{Im}\,\varepsilon}\,. \tag{6.7}$$

To optimize the regime of reflectivity tuning transparency determined by (6.6), the following circumstances have to be taken into account:

(A) The different physical mechanisms of scattering of carriers interacting with a semiconductor crystal lattice are characterized by different dependences $v(T_e)$. It makes sense to consider the conditions in which the scattering on ionized impurities prevails over other scattering mechanisms, because the scattering on ionized impurities is distinguished by the strong temperature dependence [58]

$$v(T_e) = v_0 f^{-3/2}\,, \tag{6.8}$$

where f is the normalized value of the carrier temperature T_e ($f = T_e/T_{e0}$) and T_{e0} and v_0 are the unperturbed values of the parameters T_e and v. This situation occurs, for instance, in the n-type InAs in the low-temperature range $10 \text{ K} < T_e < 120 \text{ K}$ [59].

(B) To illustrate the possibilities of thermic control of wave beams under condition (6.5), we examine the reflection of millimeter radiation with $\lambda = 3$ mm, related to one of the atmospheric transparency windows, from a InAs plate. Taking the corresponding parameter values [60] $\varepsilon_L = 12.2$, $m^* = 0.07m$, $v_0 = 2.5 \times 10^{12}$ rad s^{-1}, $N = 3 \times 10^{14}$ cm^{-3}, and considering the electron heating from $T_{e0} = 40$ K up to $T_e = 110$ K ($f = 2.75$), we can find the power reflection coefficients $|R|^2$ for the unperturbed ($f = 1$, $|R|^2 = |R_1|^2$) and perturbed ($f = 2.75$, $|R|^2 = |R_2|^2$) conductivities: $|R_1|^2 = 0.3$, $|R_2|^2 = 0.6$. Thus, even moderate heating can double the strengthening of reflectivity.

(C) The relaxation time for the electron temperature T_e under the conditions discussed is about $t_c \approx 10$ ps [62]; therefore, the intensity of the reflected wave can be doubled during the time close to its period.

This example allows us to note the problems in the search for materials characterized by appropriate values of the parameters N and T_{e0}, providing fast electro-optical modulation of reflectivity in the spectral range between microwaves and far IR radiation and, in particular, in the submillimeter range, which is very important for applications.

6.3 Telegraph equation for a transmission line with time-varying losses
The saturation of absorption due to cross-modulation of EM waves considered in Section 6.1 corresponds to the case where both real and imaginary parts of dielectric permeability (6.6) depend on the absorption parameters. In contrast, we now discuss another model of media with time-varying conductivity, describing a series of physically meaningful situations. The well-known problem giving rise to this model is connected with the propagation of an EM wave in a transmission line with losses, described by Eqns (4.28). To stress the effects caused by time-dependent losses, we consider, for example, the growth of leakage currents produced by an increasing discharge in the line. In this way, the parameter G in (4.28), characterizing the leakage currents, is supposed to be time-dependent:

$$G = G_0\,P(t)\,, \qquad P\Big|_{t=0} = 1\,. \tag{6.9}$$

For simplicity, the resistance R is neglected below.

Expressing the voltage and current in the line in terms of the generating function ψ in (4.30), we can reduce system (4.28) to one equation, coinciding formally with the telegraph

equation with a time-varying conductivity:

$$\frac{\partial^2 \psi}{\partial z^2} - \frac{1}{v_0^2}\frac{\partial^2 \psi}{\partial t^2} = \frac{P(t)}{v_0^2 T}\frac{\partial \psi}{\partial t}, \qquad T = \frac{C}{G_0}. \tag{6.10}$$

Here, C is the capacity per unit length of the line and the velocity v_0 is defined in (4.31). The time-dependent coefficient $P(t)$ on the right side of (6.10) is an unknown function of time. To determine the function that allows an exact analytic solution of (6.10), we seek the solution in the form

$$\psi = F \exp\left[-\int_0^t \alpha(t')\,\mathrm{d}t'\right]. \tag{6.11}$$

Substitution of (6.11) in telegraph equation (6.10) gives the equation for the function F:

$$\frac{\partial^2 F}{\partial z^2} - \frac{1}{v_0^2}\frac{\partial^2 F}{\partial t^2} = \frac{1}{v_0^2}\left(MF + B\frac{\partial F}{\partial t}\right),$$

$$M = \alpha^2 - \frac{\partial \alpha}{\partial t} - \frac{\alpha P}{T}, \qquad B = \frac{P}{T} - 2\alpha. \tag{6.12}$$

Imposing the additional conditions

$$M = 0, \qquad B = \mathrm{const} = \frac{1}{t_0}, \tag{6.13}$$

we can reduce Eqn (6.12) to the standard form of the telegraph equation with constant coefficients:

$$\frac{\partial^2 F}{\partial z^2} - \frac{1}{v_0^2}\frac{\partial^2 F}{\partial t^2} = \frac{1}{v_0^2 t_0}\frac{\partial F}{\partial t}. \tag{6.14}$$

The meaning of the parameter t_0, which has the dimension of time, is to be established below.

We now seek the time dependence of leakage losses $P(t)$ and the function $\alpha(t)$ in Eqn (6.12). Representing the function $\alpha(t)$ in (6.12) as

$$\alpha = \frac{1}{2t_0}(\gamma P - 1), \qquad \gamma = \frac{t_0}{T}, \tag{6.15}$$

and substituting expression (6.15) in the condition $M = 0$ [see (6.12)], we obtain the equation for the function $P(t)$:

$$2t_0 \gamma \frac{\partial P}{\partial t} = 1 - \gamma^2 P^2. \tag{6.16}$$

The solution of Eqn (6.16) satisfying the initial conduction $P(0) = 1$ can be written in either of two forms:

$$P_1 = \left[\gamma \tanh\left(\mathrm{artanh}\,\gamma^{-1} + \frac{t}{2t_0}\right)\right]^{-1}, \quad \gamma \geqslant 1, \quad (6.17)$$

$$P_2 = \gamma^{-1}\tanh\left(\mathrm{artanh}\,\gamma + \frac{t}{2t_0}\right), \qquad \gamma \leqslant 1, \tag{6.18}$$

$$P = 1, \qquad \gamma = 1,$$

depending on the ratio between the times t_0 and T. In time $t \gg 2t_0$, the functions $P_{1,2}$ reach their asymptotic values γ^{-1}. We see from expressions (6.17) and (6.18) that the time scale t_0 characterizes the relaxation time of variable losses and the asymptotic value of the leakage parameter $G = 1/t_0$. Figure 6, representing models (6.17) and (6.18),
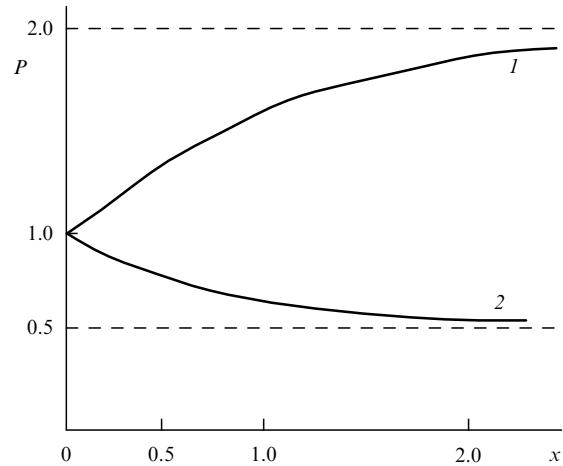

Figure 6. The normalized time-varying conductivity P in (6.17) and (6.18) as a function of time, $x = t/t_0$. Curves *1* and *2* correspond to the respective values $\gamma = 0.5$ and $\gamma = 2$.

shows the saturation of losses, which increase (decrease) with time when $\gamma > 1$ ($\gamma < 1$).

Now we can construct the function ψ in (6.11), which describes the field in a nonstationary conductor. The solution of telegraph equation (6.10) can be written as a damping wave,

$$F = \exp\left[\mathrm{i}(qz - \omega t)\right], \qquad q = \omega v^{-1}N, \qquad N^2 = 1 + \frac{\mathrm{i}}{\omega t_0}. \tag{6.19}$$

Substituting the values of $P(t)$ from (6.17) and (6.18) and then calculating the exponential factor in expression (6.11), we obtain, for instance, for the fast relaxation ($\gamma < 1$) that

$$\exp\left(-\int_0^t \alpha\,\mathrm{d}t'\right) = \frac{\exp\left[t/(2t_0)\right]}{\sqrt{1 + \gamma^2}}\left[\cosh\left(\mathrm{artanh}\,\gamma + \frac{t}{2t_0}\right)\right]^{-1}. \tag{6.20}$$

By combining results (6.19) and (6.20), we arrive at a simple solution of nonstationary telegraph equation (6.10):

$$\psi = 2\Delta^{-1}\exp\left[\mathrm{i}(qz - \omega t)\right],$$

$$\Delta = 1 + \gamma + (1 - \gamma)\exp\left(-\frac{t}{t_0}\right). \tag{6.21}$$

Substitution of the generating function ψ given by (6.21) in (4.30) gives explicit expressions for the current I and voltage V in the transmission line with time-varying leakage. The generalization of this analysis to the case of a finite resistance R is trivial.

It is interesting to note the special case of the model under discussion that corresponds to the value $B = 0$ in system of equations (6.12). In this case, Eqn (6.12) for the function F becomes the wave equation in free space,

$$\frac{\partial^2 F}{\partial z^2} - \frac{1}{v^2}\frac{\partial^2 F}{\partial t^2} = 0. \tag{6.22}$$

The solution of this equation is an arbitrary twice differentiable function $F(t - z/v)$. The function $P(t)$ determined from the conditions $M = 0$, $B = 0$ decreases according to the

formula

$$P = \left(1 + \frac{t}{2T}\right)^{-1} . \tag{6.23}$$

Calculating the exponential factor in the function F in (6.11) for model (6.23), we obtain the solution of the telegraph equation describing the propagation of an arbitrarily shaped pulse F:

$$\psi = \left(1 + \frac{t}{2T}\right) F\left(\frac{t - z/v}{t_0}\right) .$$

Substitution of (6.21) in (4.30) allows us to find both current and voltage waveforms of the EM pulse propagating in a nonstationary line with the decreasing leakage parameter $G = G_0 \left(1 + t/(2T)\right)^{-1}$.

It is worth mentioning that the analysis of the nonstationary telegraph equation developed here may also become useful for certain problems in cross-disciplinary physics. Thus, it was shown in Ref. [61] that the model of random walk with a variable speed $v = v_0 U(t)$ can be reduced to Eqn (6.10) with $P(t) = 1/U(t)$; the function then has the meaning of probability density. If the time of field variation is sufficiently long $(tP(t) \gg T)$, Eqn (6.10) is reduced to the equation governing the quasistationary field,

$$\frac{\partial^2 \psi}{\partial z^2} = \frac{P(t)}{v^2 T} \frac{\partial \psi}{\partial t} . \tag{6.24}$$

In this case, changing the time variable as

$$\tau(t) = \int_0^t \frac{\mathrm{d}t'}{P(t')} \tag{6.25}$$

converts Eqn (6.24) into the standard quasistationary equation describing, for instance, the diffusion of a field in the (z, τ) space with the diffusion coefficient equal to $v^2 T$.

7. Conclusion. Time-domain optics of unharmonic waves

In conclusion, it is worth noting some consequences of the discussed results and mentioning the problems that remain insufficiently elaborated. Attention was given above to the drastic reshaping of both reflected and refracted waves interacting with time-varying media; in particular, this interaction was shown to transform harmonic waves to unharmonic ones. Performing the relevant generalizations of reflection – refraction laws, one could speak about the optics of nonsinusoidal waves.

However, other types of nonsinusoidal waves can arise in a stationary medium or even in a free space due to coupled spatiotemporal variations in diffracted pulses. Advances over the last decade in few-cycle transient generation using broadband radars with the transient duration t_0 about 1 ns [62], terahertz optical devices ($t_0 \sim 0.1 - 1$ ps) [63], and femtosecond optical systems ($t_0 \sim 5 - 10$ fs) [64] have attracted great interest in radiophysics and optoelectronics. To examine the fast interaction of these transients with continuous media, one has to take the spatiotemporal evolution of transients on the way from source to target into account. To understand the fundamental role of coupling between spatial and temporal reshaping of the pulse, it is worthwhile to show, first, how

these processes develop during paraxial propagation of a three-dimensional pulse in a free space (Section 7.1); a flexible model of waveforms characterized by a well-expressed leading edge with a finite slope, an arbitrary number of unharmonic oscillations, and an exponentially damping 'tail' is described in Section 7.2. The effects of diffraction – dispersion coupling, including pulse reshaping, frequency red-shifting, and polarity reversal for a pulse traveling in a dispersive medium, are considered in Section 7.3.

7.1 Diffraction-induced spatiotemporal evolution of pulses in a free space

The interplay between transverse, longitudinal, and temporal distortions of localized pulses traveling in the z-direction is described by the paraxial equation for the electric field $E(\mathbf{r}, z, t)$ [65]:

$$\Delta_\perp E = \frac{2}{c} \frac{\partial^2 E}{\partial z \, \partial t'} , \qquad \Delta_\perp = \frac{\partial^2}{\partial x^2} + \frac{\partial^2}{\partial y^2} , \qquad t' = t - \frac{z}{c} . \tag{7.1}$$

The nonseparable solution of Eqn (7.1) is

$$E(\mathbf{r}, z, t') = \frac{\mathrm{i}L_R}{q} F\left(t' - \frac{r^2}{2cq}\right) , \tag{7.2}$$

where $r^2 = x^2 + y^2$, $q = z + \mathrm{i}L_R$,

$$L_R = \frac{k a_0^2}{2} \tag{7.3}$$

is the diffraction length, k is the wavenumber, a_0 is the waist radius of the paraxial beam, and F is an arbitrary function. The pulsed beam diffraction arising due to its finite transverse size induces, through the factor $\mathrm{i}L_R/q$ in Eqn (7.2), the propagation changes in the on-axis waveform. Writing this factor as

$$\frac{\mathrm{i}L_R}{q} = \frac{\exp{(\mathrm{i}\varphi)}}{\sqrt{1 + (z/L_R)^2}} , \qquad \varphi = \arctan\left(\frac{z}{L_R}\right) , \tag{7.4}$$

we can relate the factor $\left[1 + (z/L_R)^2\right]^{-0.5}$ to the pulse amplitude attenuation, while the phase φ is responsible for the evolution of the pulse shape: Eqn (7.2) is real at $z = 0$ and imaginary for large $z \gg L_R$. The parameter in (7.4) is known as the Gouy phase shift and takes values from -0.5π to $+0.5\pi$. Independent of the choice of the function F, the coupling of its spatial and temporal variations comes from the complex space-dependent time shift $r^2/(2cq)$. Its real part

$$t_s = -\frac{z r^2}{2c|q|^2} \tag{7.5}$$

is the actual time of arrival of the pulse at each plane z. This shift is connected with the paraxial spherical phase front of radius $R(z)$:

$$R(z) = \frac{|q|^2}{2} = z\left[1 + \left(\frac{L_R}{z}\right)^2\right] . \tag{7.6}$$

The imaginary part of the time shift, $\mathrm{i}L_R r^2/(2c|q|^2)$, determines the spatial distribution of pulse attenuation.

We illustrate the spatiotemporal coupling phenomena by choosing the function F in the form of a few-cycle three-dimensional pulsed wave beam described by the so-called
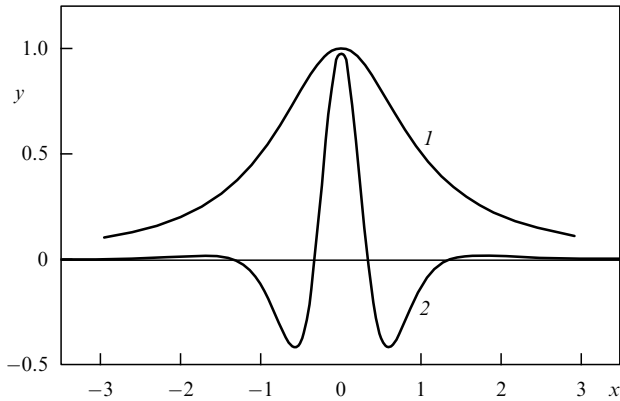
Figure 7. Poisson-spectrum pulses (7.7) for the parameter values $m = 1$ (curve *1*) and $m = 2$ (curve *2*) are plotted vs the normalized time $x = t/t_0$.

Poisson-spectrum pulse [66]:

$$F = \operatorname{Re} f(t), \quad f(t) = \left(1 - \frac{\mathrm{i}t'}{t_0}\right)^{-m}. \tag{7.7}$$

Here, t_0 and the integer $m \geqslant 1$ are free parameters and $t' = t - z/c$ is the retarded time for points located on the z axis ($x = 0, y = 0$). This nonseparable waveform, depicted in Fig. 7, provides a useful analytic tool for the investigation of coupled diffraction- and dispersion-induced distortions of localized fields with curvilinear wavefronts.

We stress some important properties of Poisson-spectrum pulses.

(A) This flexible model is suitable for waveforms of any duration and with an arbitrary number of oscillations.

(B) The $1/e$ width of this pulse is

$$T = t_0 \sqrt{\exp\left(\frac{2}{m}\right) - 1}, \tag{7.8}$$

which can represent a large variety of pulses: the value $m = 1$ is related to a single maximum of F, whereas large values of the parameter m correspond to a growing number of oscillations with an almost constant frequency $\omega = m/t_0$ in the central part of the pulse. The limit $m \gg 1$ is related to the cos-Gaussian pulse

$$F = \exp\left(-\frac{t^2}{T^2}\right) \cos(\omega t).$$

(C) To describe the dynamics of a three-dimensional structure of pulses (7.7), we must replace the retarded time t' by the shifted time $t' - r^2/(2cR)$, where R and r are the radius of wavefront curvature (7.6) and the distance between the beam axis and the observation point on the wavefront.

To examine the formation of a spatiotemporal structure from waveform (7.7) in the course of its propagation, we can rewrite solution (7.2) with the above-mentioned replacements $t' \to t' - r^2/(2cR)$:

$$E(\mathbf{r}, z, t') = \frac{\mathrm{i}L_R}{q} \left[\frac{\mathrm{i}t_0}{t' - r^2/(2cR) + \mathrm{i}\left(t_0 + r^2 L_R/(2c|q|^2)\right)} \right]^m. \tag{7.9}$$

According to definition (7.7), we must use the real part of (7.9).
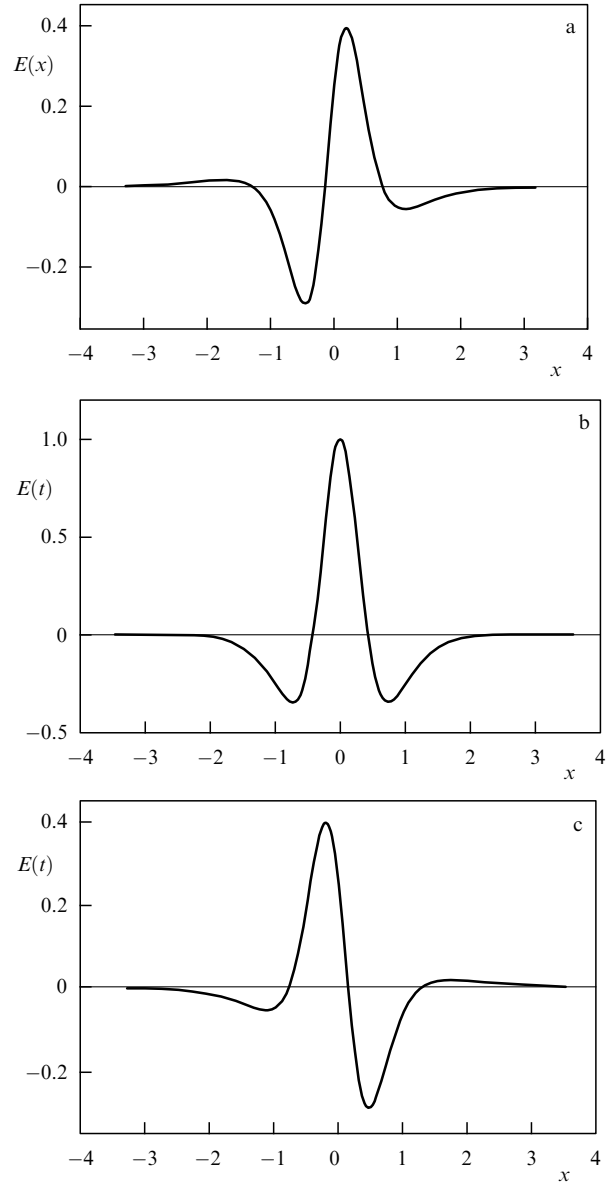
Figure 8. Reshaping of Poisson-spectrum pulse (7.7) with $m = 4$ and reversal of its polarity on the beam axis in the course of propagation from $z = -2L_R$ (a), through $z = 0$ (b), and further to $z = 2L_R$ (c).

Solution (7.9) reveals the following spatiotemporal distortions of the initial waveform:

(1) The $1/e$ pulse width is increased compared with (7.8):

$$T = t_0\left(1 + \frac{r^2 L_R}{2c|q|^2}\right) \sqrt{\exp\left(\frac{2}{m}\right) - 1}. \tag{7.10}$$

(2) The frequency of oscillations is red-shifted:

$$\omega_m = m\left(t_0 + \frac{r^2 L_R}{2c|q|^2}\right)^{-1}. \tag{7.11}$$

(3) The Gouy factor $\mathrm{i}L_R/q$ describes pulse temporal reshaping, including its polarity reversal during pulse travel from $z \ll -L_R$ to $z \gg L_R$ (Fig. 8).

Such transformations have been observed experimentally in the diffraction of ultrashort pulses [67].

7.2 Modeling of unharmonic transients
by means of Laguerre functions

The effects of spatiotemporal reshaping of a pulse in a free space were shown above by means of a simple model of a Poisson-spectrum pulse. However, the dynamics of such reshaping depend on the pulse waveform, which can differ essentially from the traditional models of quasimonochromatic signals with rectangular or Gaussian envelops:

(a) the ultrashort transient contains only a few field cycles, whose shape is usually far from sinusoidal;

(b) the rising and falling edges of the transient are asymmetric;

(c) the zeros of the envelop are unequally spaced.

Flexible models of plane-wave envelops describing continuous waveforms that have properties (a)–(c) can be represented by a series of Laguerre functions $L_n(t')$ defined on the time interval $0 \leqslant t < \infty$ [32],

$$F(t') = \sum_{n=0}^{\infty} a_n L_n(t') . \tag{7.12}$$

The Laguerre functions

$$L_n(x) = \frac{\exp(x/2)}{n!} \frac{\mathrm{d}^n}{\mathrm{d}x^n} \left[x^n \exp(-x) \right] \tag{7.13}$$

are known to be orthonormal on the interval $0 \leqslant x < \infty$,

$$\int_0^{\infty} L_n(x)\, L_m(x)\, \mathrm{d}x = \delta_{nm} . \tag{7.14}$$

The behavior of the L_n near the leading edge of the transient $x \to 0$ (Fig. 9a),

$$L_n(0) = 1 , \qquad \frac{\partial L_n(x)}{\partial x}\bigg|_{x=0} = -\left(n + \frac{1}{2}\right) , \tag{7.15}$$

shows that none of the functions L_n can themselves represent a signal with zero starting point. However, such a signal can be represented by linear combination (7.12) obeying the condition

$$\sum_{n=0}^{\infty} a_n = 1 . \tag{7.16}$$

The simplest example of the discussed waveform, given by expression (7.12),

$$F_m(t') = B\left[L_m(t') - L_{m+2}(t') \right] , \tag{7.17}$$

is shown in Fig. 9b in the case where $m = 0$, $a_0 = 1$, and $a_2 = -1$, the other coefficients in (7.12) being zeros. To compare waveforms (7.17) with different values of m, the waveforms corresponding to the values $m = 0$, 1, and 2, are depicted in Fig. 9b.

Waveforms (7.17) have a number of properties suitable for modeling single-cycle and few-cycle transients:

(1) Unlike the Gaussian and Poisson-spectrum pulses, extended from $-\infty$ to $+\infty$, the waveforms F_m in (7.17) have a well-expressed leading edge at the point $t = 0$ and a controlled slope at this point:

$$F_m(0) = 0 , \qquad \frac{\partial F_m}{\partial t'}\bigg|_{t'=0} = \frac{2B}{t_0} . \tag{7.18}$$

(2) The waveforms F_m can contain an arbitrary number of unharmonic oscillations. The temporal structure of the waveform F_m has $m+2$ zero-crossing points, spaced by unequal distances, $m+2$ different extrema, and an exponentially decreasing 'tail'.

(3) The envelope F_m has the integral property

$$\int_0^{\infty} F_m(x)\, \mathrm{d}x = 0 . \tag{7.19}$$

Until now, we have been discussing plane waves. However, using the procedure applied in Section 7.1 to the Poisson-spectrum pulses, we can build the three-dimensional solution of Eqn (7.1) related to the Laguerre waveforms F_m, in the form of nonseparable solution (7.2):

$$E(\mathbf{r}, z, t) = \frac{\mathrm{i}L_R}{q}\, F_m(u) , \qquad u = \frac{t' - r^2/(2cq)}{t_0} . \tag{7.20}$$

After this, the tendencies of the space–time evolution of pulses in a free space, visualized in Section 7.1 for the model of a Poisson-spectrum pulse, can also be revealed for the transients F_m; however, more tedious algebra is needed for the analysis of F_m.
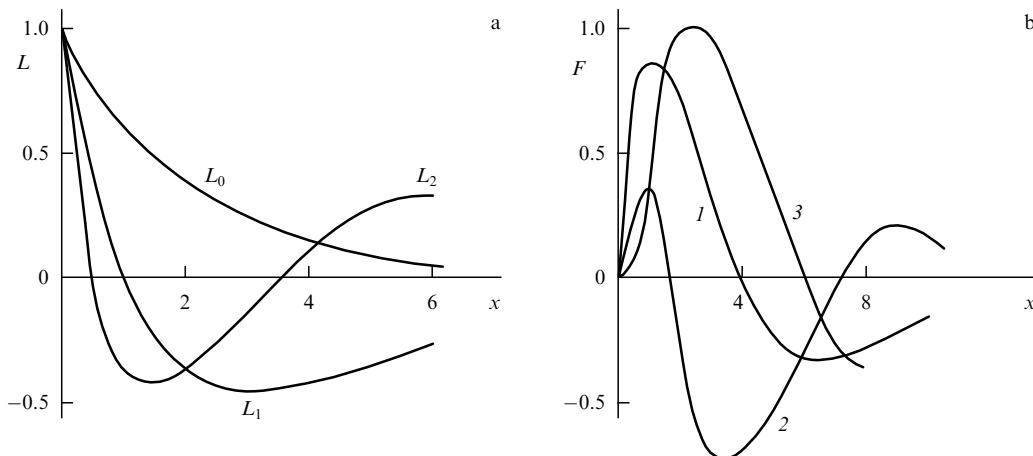
Figure 9. (a) Laguerre envelops $L_0(x)$, $L_1(x)$, and $L_2(x)$; (b) curves *1*, *2*, and *3* correspond to the respective envelopes F_0, F_1, and F_2 (7.17); $x = t/t_0$.

The tendencies of formation of unharmonic waves were discussed above in the framework of the model of a dispersionless homogeneous medium. Manifestations of the same tendencies in a dispersive medium result in the enrichment of this process by new phenomena.

7.3 Nonstationary waves in stationary media

The dynamics of unharmonic waveforms with curvilinear phase fronts in dispersive media depend on the interplay of diffraction and dispersion perturbations. The mathematical basis for the analysis of dispersive effects in paraxial CW Bessel beams and Gaussian pulse beams was developed in Refs [68, 69]. Avoiding the massive mathematical computations used in these articles, we qualitatively mention the physical fundamentals of these processes. The most significant space–time coupling phenomena arising due to the interaction of diffractive and dispersive effects are related to the curvature of the pulse front. In the course of propagation, the redder frequencies, diffracted at large angles and therefore traveling at a reduced longitudinal velocity, are delayed with respect to the bluer frequencies, diffracted at smaller angles. On the other hand, there is an additional pulse front curvature in dispersive media, originated by the difference of group velocities between the on-axis part of the pulse and the off-axis red-shifted part. In normal dispersion, the red components, diffracted further from the axis, travel faster than the blue components near the axis, while the opposite occurs in anomalous dispersion. The normal dispersion straightens out the pulse fronts, bending them in the opposite direction to that of the diffraction-induced one; in the anomalous dispersion, both curvatures add up.

This spatial separation of frequencies arising between the on-axis and off-axis parts of a diffracting pulse can become interesting for the control of pulse angular divergence. The dynamics of reshaping processes in pulsed beams are governed by the competition between diffraction, increasing the pulse front curvature, and dispersion, connected with the frequency red-shift at the off-axis part of the pulse. The curvature radius of the pulse front, arising due to the superposition of diffraction- and dispersion-induced curvatures, was obtained for Gaussian pulsed beams as [66]

$$\frac{1}{R_T} = \left(1 \mp \frac{L_R}{L_D}\right) \frac{1}{R}, \tag{7.21}$$

where R is the curvature radius in a free space, Eqn (7.6), L_R is diffraction length (7.3), the signs '−' ('+') in (7.21) correspond to the normal (abnormal) dispersion, and L_D is the dispersion length dependent on some characteristic pulse duration:

$$L_D = \frac{2(\Delta t)^2}{|K_{\omega\omega}|}, \qquad K_{\omega\omega} = \frac{\partial^2 K}{\partial \omega^2}. \tag{7.22}$$

We see from (7.21) that normal dispersion can weaken the wavefront convexity and even make it concave. In the special case where $L_R = L_D$, the wavefront remains planar in the model under discussion.

To illustrate the feasibility of controlled variation of the pulse front curvature, we evaluate the parameters in formula (7.21). We consider the Gaussian pulse with the half-width $\Delta t = 1.4$ fs and carrier frequency $\omega = 1.75 \times 10^{15}$ rad s^{-1} ($\lambda = 1.06$ μm) traveling in a fused silica; the wavenumber k and the value $K_{\omega\omega}$ are $k = 91.930$ cm^{-1} and $K_{\omega\omega} = 217.8$ cm^{-1} fs^2; and the dispersive length L_D is

1.8×10^{-3} cm. Supposing the initial beam width a_0 in (7.3) to be 2, 6.3, and 19 μm, we have the ratio L_R/L_D equal to 0.1, 1, and 10, respectively. In the case of a small waist size ($L_R/L_D = 0.1$), diffraction is much stronger than dispersion, and the pulse fronts remain convex. In the case where $a_0 = 6.3$ μm, the dispersion cancels the diffraction curvature. Finally, in the case where $a_0 = 19$ μm ($L_R/L_D = 10$), the stronger dispersion turns the pulse front concave.

It was supposed above that the diffracted pulse incident on the interface of a dispersive medium is characterized by a spherical phase front. Strictly speaking, the spatiotemporal structure of the incident pulse in a far zone is determined by the generalized time-dependent diffraction integral [70]

$$E(x, y, z, t) = \frac{1}{c} \iint \frac{\partial}{\partial t} E_0\left(x', y', 0, t - \frac{z}{c}\right) \frac{z}{R^2}\, dx'\, dy', \tag{7.23}$$

where $R^2 = x^2 + y^2 + z^2$. According to (7.23), the diffracted pulse can be split into two partially overlapping pulses if the observation angle is sufficiently large [68]. The shorter the pulse, the deeper the minimum resulting from its splitting. However, the problem of controlled interaction of such complicated waveforms with dispersive media has not yet been examined.

Propagation of electromagnetic waves in nonstationary media was examined above by means of exact analytic solutions of the Maxwell equations for these media. Generalization of the classical Fresnel formulas based on these solutions had shown the decisive role of nonstationarity-induced dispersion in the whole set of reflection–refraction processes in time-varying media. The dynamical regimes of reflectivity resulting in spectral broadening and ultrafast amplitude–phase reshaping of EM waves are analyzed in the framework of exactly solvable models of time-dependent dielectric permeability; the special models describing these effects for rapidly ionizing plasmas are presented. The properties of unharmonic waves forming in time-varying media are visualized owing to a special mathematical transformation, reducing these waves to harmonic ones in some conventional space. Qualitative analogies between nonstationary dielectrics and transmission lines with time-varying parameters are widely used.

The electrodynamics of nonstationary media is nowadays a 'hot' and rapidly expanding branch of wave theory. However, it is worth stressing some problems that still remain today.

(1) The optics of media with moving spatiotemporal perturbations of the refractive index.

(2) The search for optimized regimes for the propagation of directed beams of single-cycle transients through nonstationary media.

(3) The nonstationary electrodynamics of random media.

(4) The time-domain analysis of ultrafast optical phenomena.

(5) The development of the quantum approach to nonstationary optical problems explaining, in particular, the generation of photons in squeezed states due to nonadiabatic distortions of the electromagnetic vacuum (see, e.g., Refs [12, 58] and the references therein).

Experimental methods in the optics of nonstationary media are now in the making. To develop these methods, one needs high temporal resolution for the observation of rapid wave processes and short-lived states of matter in the

picosecond and femtosecond ranges. Unlike the electronic technique used for measuring short radio pulses irradiated by UBW radars [71], similar measurements of light fields require new broadband optical systems. Such systems have been used successfully, for example, for observing spectra of relaxation oscillations of molecules in the THz range [72] and measuring pulse electric fields by means of spectral-phase interferometry [73]. Growing attention is being given now to the unique properties of nonstationary optical fields arising due to the interaction of laser radiation with rapidly ionizing plasmas with the ionization time shorter than the pumping wave period, and, in particular, to the generation of the high harmonics ($n > 200$) of this wave [74]. The elaboration of such methods provides the experimental basis for a new branch in the optics of nonstationary media — attosecond optics [75].

Acknowledgements

References

1. Ginzburg V L *Izv. Akad. Nauk SSSR Ser. Fiz.* **12** 393 (1948)
2. Morgenthaler F R *IEEE Trans. Microwave Theory Techn.* **MTT-6** 167 (1958)
3. Salieres S et al., in *Advances in Atomic, Molecular and Optical Physics* Vol. 41 (Eds B Bederson, H Walther) (New York: Academic Press, 1999) p. 83
4. Geindre J-P et al. *Opt. Lett.* **26** 1612 (2001)
5. Bertolotti M, Ferrari A, Sereda L *J. Opt. Soc. Am. B* **12** 1519 (1995)
6. Kaplan A E *J. Opt. Soc. Am. B* **15** 951 (1998)
7. Kuo S P, Ren A *IEEE Trans. Plasma Sci.* **PS-21** 53 (1993)
8. Rayleigh J W S *Proc. London Math. Soc.* **11** 51 (1880)
9. Felsen L, Whitman G *IEEE Trans. Antennas Propag.* **AP-18** 242 (1970)
10. Mendonça J T, Guerreiro A, Martins A M *Phys. Rev. A* **62** 033805 (2000)
11. Abeles F, in *Progress in Optics* Vol. 2 (Ed. E Wolf) (Amsterdam: North-Holland, 1963) p. 249
12. Dodonov V V, Klimov A B, Nikonov D E *Phys. Rev. A* **47** 4422 (1993)
13. Kuo S P *Phys. Rev. Lett.* **65** 1000 (1990)
14. Joshi C J et al. *IEEE Trans. Plasma Sci.* **PS-18** 814 (1990)
15. Kalluri D K, Goteti V R *J. Appl. Phys.* **72** 4575 (1992)
16. Banos A (Jr), Mori W B, Dawson J M *IEEE Trans. Plasma Sci.* **PS-21** 57 (1993)
17. Mendonca J T, Oliveira e Silva L *IEEE Trans. Plasma Sci.* **PS-24** 147 (1996)
18. Niikura H et al. *Nature* **417** 917 (2002)
19. Oliveira e Silva L, Mendonca J T *IEEE Trans. Plasma Sci.* **PS-24** 503 (1996)
20. Schiff L I *Quantum Mechanics* 3rd ed. (New York: McGraw-Hill, 1968) [Translated into Russian (Moscow: IL, 1959)]
21. Yu W et al. *J. Phys. D: Appl. Phys.* **26** 2093 (1993)
22. Savage R L (Jr), Joshi C, Mori W B *Phys. Rev. Lett.* **68** 946 (1992)
23. Esarey R E, Joyce G, Sprangle P *Phys. Rev. A* **44** 3908 (1991)
24. Koretzky E, Kuo S P, Kim J *J. Plasma Phys.* **59** 315 (1998)
25. Ogusu K *J. Opt. Soc. Am. B* **17** 1894 (2000)
26. Wilks S C et al. *Phys. Rev. Lett.* **62** 2600 (1989)
27. Kapteyn H C, Murnane M M *J. Opt. Soc. Am. B* **8** 1657 (1991)
28. Mori W B *Phys. Rev. A* **44** 5118 (1991)
29. Mendonça J T, Oliveira e Silva L *Phys. Rev. E* **49** 3520 (1994)
30. Dias J M et al. *Phys. Rev. Lett.* **78** 4773 (1997)
31. Oliveira e Silva L, Mendonca J T *IEEE Trans. Plasma Sci.* **PS-24** 316 (1996)
32. Shvartsburg A, Petite G, in *Progress in Optics* Vol. 44 (Ed. E Wolf) (Amsterdam: Elsevier Sci., 2002) p. 143
33. Bernstein I, in *Handbook of Plasma Physics* Vol. 1 (Eds M Rosenbluth, R Sagdeev) (Amsterdam: North-Holland, 1983) p. 367
34. Shvartsburg A B *Impulse Time-Domain Electromagnetics of Continuous Media* (Boston: Birkhäuser, 1999)
35. Abramowitz M, Stegun I A (Eds) *Handbook of Mathematical Functions, with Formulas, Graphs, and Mathematical Tables* (New York: Dover Publ., 1965) [Translated into Russian (Moscow: Nauka, 1979)]
36. Kapteyn H C et al. *Opt. Lett.* **16** 490 (1991)
37. Gold D M *Opt. Lett.* **19** 2006 (1994)
38. Teubner U et al. *Phys. Rev. A* **67** 013816 (2003)
39. Chwalek J M et al. *Appl. Phys. Lett.* **57** 1696 (1990)
40. Fedorov M V *Elektron v Sil'nom Svetovom Pole* (Electron in the Powerful Light Field) (Moscow: Nauka, 1991) [Translated into English (Singapore: World Scientific, 1991)]
41. Born M, Wolf E *Principles of Optics* 6th ed. (Oxford: Pergamon Press, 1980) [Translated into Russian (Moscow: Nauka, 1970)]
42. Jiang Z, Jacquemin R, Eberhardt W *Appl. Opt.* **36** 4358 (1997)
43. Eesley G L et al. *Phys. Rev. Lett.* **65** 3445 (1990)
44. Jackson J D *Classical Electrodynamics* 2nd ed. (New York: Wiley, 1975) [Translated into Russian (Moscow: Mir, 1965)]
45. Tang N, Sutherland R L *J. Opt. Soc. Am. B* **14** 3412 (1997)
46. Shvartsburg A B, Petite G, Hecquet P *J. Opt. Soc. Am. A* **17** 2267 (2000)
47. Ginzburg V L *Rasprostranenie Elektromagnitnykh Voln v Plazme* (The Propagation of Electromagnetic Waves in Plasmas) (Moscow: Nauka, 1967) [Translated into English (Oxford: Pergamon Press, 1970)]
48. Stenflo L, Shvartsburg A B, Weiland J *Contrib. Plasma Phys.* **37** 393 (1997)
49. Musielak Z E, Fontenla J M, Moore R L *Phys. Fluids B* **4** 13 (1992)
50. Loka H S, Benjamin S D, Smith P W E *IEEE J. Quantum Electron.* **34** 1426 (1998)
51. Åberg I, Kristensson G, Wall D J N *J. Math. Phys.* **37** 2229 (1996)
52. Méplan O, Gignoux C *Phys. Rev. Lett.* **76** 408 (1996)
53. Cirone M, Rzazewski K, Mostowski J *Phys. Rev. A* **55** 62 (1997)
54. Law C K, Eberly J H *Phys. Rev. Lett.* **76** 1055 (1996)
55. Landau L D, Lifshitz E M *Mekhanika* (Mechanics) (Moscow: Nauka, 1973) [Translated into English (Oxford: Pergamon Press, 1976)]
56. Mattos M A da F, Christopoulos C *J. Phys. D: Appl. Phys.* **23** 40 (1990)
57. Raizer Yu P *Fizika Gazovogo Razryada* (Gas Discharge Physics) (Moscow: Nauka, 1987) [Translated into English (Berlin: Springer-Verlag, 1991)]
58. Moss T S (Ed.) *Handbook on Semiconductors* Vol. 2 (Amsterdam: North-Holland Publ. Co., 1980)
59. Anderson D A, Apsley N *Semicond. Sci. Technol.* **1** 187 (1986)
60. Winnerl S et al. *Phys. Status Solidi B* **204** 58 (1997)
61. Masoliver J, Weiss G H *Phys. Rev. E* **49** 3852 (1994)
62. Samaddar S, Mokole E, in *Ultra-Wideband, Short-Pulse Electromagnetics 3* (Eds C E Baum, L Carin, A P Stone) (New York: Plenum Press, 1997) p. 147
63. McGowan R W, Gallot G, Grischkowsky D *Opt. Lett.* **24** 1431 (1999)
64. Brabec T, Krausz F *Rev. Mod. Phys.* **72** 545 (2000)
65. Einziger P D, Raz S *J. Opt. Soc. Am. A* **4** 3 (1987)
66. Porras M A *Phys. Rev. E* **58** 1086 (1998)
67. Feng S, Winful H G, Hellwarth R W *Opt. Lett.* **23** 385 (1998)
68. Porras M A *Opt. Lett.* **26** 44 (2001)
69. Porras M A *J. Opt. Soc. Am. B* **16** 1468 (1999)
70. Wang Z, Xu Z, Zhang Z *Opt. Lett.* **22** 354 (1997)
71. Guo Y, Überall H *J. Electromagn. Waves Appl.* **8** 355 (1994)
72. Mokhtari A E A, Chesnoy J *IEEE J. Quantum Electron.* **25** 2528 (1989)
73. Iaconis C, Walmsley A *Opt. Lett.* **23** 792 (1998)
74. Corkum P B *Phys. Rev. Lett.* **71** 1994 (1993)
75. Paul P M et al. *Science* **292** 1689 (2001)